Am J Cancer Res 2022;12(1):427-444
www.ajcr.us /ISSN:2156-6976/ajcr0140703

Original Article

Guanosine primes acute myeloid leukemia for differentiation via guanine nucleotide salvage synthesis

Hanying Wang[1,2], Xin He[2], Zheng Li[2], Hongchuan Jin[3], Xian Wang[1], Ling Li[2]

[1]Department of Medical Oncology, Sir Run Run Shaw Hospital, School of Medicine, Zhejiang University, Hangzhou 310016, Zhejiang, China; [2]Department of Hematological Malignancies Translational Science, Gehr Family Center for Leukemia Research, Beckman Research Institute, City of Hope National Medical Center, Duarte, CA 91010, USA; [3]Laboratory of Cancer Biology, Key Lab of Biotherapy in Zhejiang Province, Cancer Center of Zhejiang University, Sir Run Run Shaw Hospital, School of Medicine, Zhejiang University, Hangzhou 310016, Zhejiang, China

Received November 22, 2021; Accepted December 27, 2021; Epub January 15, 2022; Published January 30, 2022

Abstract: Differentiation arrest represents a distinct hallmark of acute myeloid leukemia (AML). Identification of differentiation-induction agents that are effective across various subtypes remains an unmet challenge. GTP biosynthesis is elevated in several types of cancers, considered to support uncontrolled tumor growth. Here we report that GTP overload by supplementation of guanosine, the nucleoside precursor of GTP, poises AML cells for differentiation and growth inhibition. Transcriptome profiling of guanosine-treated AML cells reveals a myeloid differentiation pattern. Importantly, the treatment compromises leukemia progression in AML xenograft models. Mechanistically, GTP overproduction requires sequential metabolic conversions executed by the purine salvage biosynthesis pathway including the involvement of purine nucleoside phosphorylase (PNP) and hypoxanthine phosphoribosyltransferase 1 (HPRT1). Taken together, our study offers novel metabolic insights tethering GTP homeostasis to myeloid differentiation and provides an experimental basis for further clinical investigations of guanosine or guanine nucleotides in the treatment of AML patients.

Keywords: Acute myeloid leukemia, guanosine 5'-triphosphate, myeloid differentiation, PNP, HPRT1

Introduction

Acute myeloid leukemia (AML) is a devastating malignancy characterized by differentiation arrest and aberrant self-renewal of immature myeloblasts [1]. In spite of improved therapeutic strategies guided by cytogenetic and molecular risk-adapted approaches, the chemotherapy regimen established in the 1970s remains the treatment paradigm [2], with clinical outcomes still far from satisfactory [3].

The exceptional success of all-trans retinoic acid (ATRA) and arsenic trioxide in acute promyelocytic leukemia (APL) highlighted the merits of differentiation therapy [4]. Instead of inducing cytotoxic cell death, it was coined to resume terminal differentiation of leukemic blasts and promote subsequent turnover of mature myeloid cells [5]. With advances in understanding the genomic landscape of AML, more differentiation-inducing agents have been identified in the last few decades [6]. Foremost among those emerging differentiation therapies are newly approved inhibitors of mutant isocitrate dehydrogenase 1 (IDH1) [7] or IDH2 [8], which yield functional neutrophils in ~20% of AML patients carrying IDH1/2 mutation [9-11]. However, successful legends for differentiation therapy have still been lacking within the remaining non-APL, non-IDH1/2 mutant AML patients.

Leukemic cells commonly hijack active nucleotide synthesis to fuel anabolic demands [12]. Abrogating nucleotide metabolism thus represents a promising strategy to induce AML differentiation, which may not be limited to any specific AML subgroups [13]. In fact, recent reports indicate that targeting de novo pyrimidine nucleotide synthesis [14, 15], de novo purine nucleotide synthesis [16, 17], serine syn-

thesis or one-carbon folate cycle [18-20] overcomes differentiation blockage in AML. In contrast, emerging studies also suggest a non-proliferative role of purines and pyrimidines in cancer [21, 22]. Nevertheless, the effects of those naturally occurring metabolites, including purine/pyrimidine nucleosides and nucleotides [23], on AML differentiation have been much less well understood.

Here, we revealed an unanticipated role of guanosine-5'-triphosphate (GTP) in promoting AML differentiation. Exogenous high level of GTP exerts its effects through prior degradation to guanosine for cell entry. In turn, guanosine supplementation induces differentiation through intracellular GTP overproduction. Importantly, both purine nucleoside phosphorylase (PNP) and hypoxanthine phosphoribosyltransferase 1 (HPRT1) are critical players involved in guanosine-imposed GTP salvage synthesis. Our study bridges a metabolic link between GTP and myeloid differentiation in AML and proposes pharmaceutical evaluation of guanosine or guanine nucleotides as potential differentiation-induction strategy.

Materials and methods

Cell culture

293T cells were cultured in DMEM medium with 10% FBS and 1% penicillin/streptomycin (Gibco). The human AML cell lines KG1A, KASUMI1, HL60, NB4, OCI-AML3, MOLM13, MV4-11, NOMO1, THP1, U937 (ATCC) were cultured in RPMI 1640 medium with 10% FBS and 1% penicillin/streptomycin. Human primary AML $CD34^+$ cells were maintained in StemSpan Serum-Free Expansion Media (SFEM, Stemcell Technologies, Cat# 09600) supplemented with 50 ng/mL of recombinant human stem cell factor (SCF), 100 ng/mL of Fms-like tyrosine kinase 3 ligand (Flt3L), 100 ng/mL of thrombopoietin (TPO), 25 ng/mL of interleukin 3 (IL-3), and 10 ng/mL of interleukin-6 (IL-6) (Peprotech Inc.). All the experiments were performed in culture medium supplemented with 10% heat-inactivated FBS if not otherwise indicated. For heat-inactivation, culture medium containing 10% FBS was heated in water bath for 1 h at 59°C followed by cooling to 37°C. Cells were grown at 37°C in a humidified atmosphere under 5% CO_2.

Analysis of cell viability and colony growth

AML cells were treated with different nucleotides or nucleosides (Millipore Sigma, ATP: Cat# A7699, UTP: Cat# U6750, CTP: Cat# 30320, GTP: Cat# G8877, adenosine: Cat# A4036, uridine: Cat# U3003, cytidine: Cat# C4654, guanosine: Cat# G6752) as indicated. Cell growth was measured using the Cell Titer-Glo Luminescent Cell Viability Assay Kit (Promega, Cat# G7572) in accordance with the manufacturer's instructions. Results were expressed as a percentage of control from three replicates. Colony formation capacity based on colony forming cell number was determined in methylcellulose progenitor assays as described [24, 25]. Briefly, $CD34^+$ AML specimens were seeded in 24-well plates (100,000 cells per well) and cultured in methylcellulose medium with 5 ng/mL of IL-3, 5 ng/mL of SCF, 20 ng/mL of granulocyte colony stimulating factor (G-CSF) and 20 ng/mL of granulocyte-macrophage colony-stimulating factor (GM-CSF) containing 100 μM guanosine or PBS control. Colony formation units were counted after 14 days.

Flow cytometry

Human AML cell lines or primary AML cells were seeded in 24-well plates (200,000 per well) and treated as indicated. After stained with flow cytometry antibodies (BioLegend, APC anti-human CD11b antibody, Cat# 301310 or PE/Cyanine7 anti-human CD11b antibody, Cat# 301322; PerCP/Cyanine5.5 anti-human CD14 antibody, Cat# 325622), cells were resuspended in FACS buffer containing 1 μg/mL DAPI and analyzed on LSRII or Fortessa X20 flow cytometer (BD).

RNA-Seq analysis

Total RNA was isolated from cells using Trizol Reagent (Life technologies) following the manufacturer's instructions. RNA quality (RNA integrity number [RIN]) was assessed using an Agilent Bioanalyzer, and all samples were evaluated as RIN>8. RNA sequencing libraries were prepared with Kapa RNA HyperPrep kit with polyA kit (Kapa Biosystems, Cat# KR1352) according to the manufacturer's protocol. Sequencing run was performed in the single read mode using Illumina HiSeq 2500. Sequenced reads were aligned to the human hg38 reference genome with TopHat2 (v

Table 1. Clinical information relevant to primary AML specimens (related to **Figure 3**)

ID	Type	Risk	Status	Gene mutation	Cytogenetics	WBC(k)	% Blast (PB, BM)
1	PB	P	R	ITD, NPM1	ND	62.3	88, ND
2	PB	I	U	NRAS	Inv (3)	NA	24, 30
3	BM	P	R	KRAS, NRAS, U2AF1, ITD	NK	73.5	ND, 39

Abbreviations: BM, bone marrow; PB, peripheral blood; I, intermediate-risk; P, poor-risk; U, untreated; R, relapsed; ITD, FLT3-ITD; ND, not determined; NK, normal karyotype; NA, not available.

2.0.14). Gene expression level was quantified using HTSeq (v 0.6.1). The counts data were normalized using the trimmed mean of M values (TMM) method, implemented in the Bioconductor package edgeR (v.3.30.3) to obtain the normalized RPKM (Reads Per Kilobase of transcript, per Million mapped reads) value. The differential expression analysis was also performed using edgeR (v.3.30.3). The enrichment analysis was performed using Gene Set Enrichment Analysis (GSEA, v.4.0.3) and Ingenuity Pathway Analysis (IPA, v.62089861).

In vivo bioluminescence imaging

AML cell line xenograft models of systemic disease were established as described previously [26]. Briefly, U937 cells were infected with lentiviral vectors expressing luciferase reporter plus GFP and then sorted based on GFP positivity. Luciferase-expressing U937 cells (0.5×10^6 cells per mouse) were pretreated with guanosine or PBS control as indicated before intravenous inoculation into 6-8-week-old female immunodeficient NOD-scid IL2Rgnull-3/GM/SF (NSGS) mice (Jackson Laboratory, Stock# 013062) (n=8 per group). For in vivo bioluminescence imaging, mice were injected intraperitoneally with 150 mg/kg D-luciferin (Goldbio, Cat# LUCK-3G) dissolved in PBS solution, and then anesthetized with isoflurane, followed by imaged with Lago X (Spectral Instruments Imaging). The bioluminescent signals were quantified using Aura imaging software (Spectral Instruments Imaging). Total flux values were determined by drawing regions of interest and are presented as photons/second/cm^2/steradian.

Patient samples

Peripheral blood or bone marrow samples were obtained from AML patients at City of Hope (COH) Comprehensive Cancer Center. Patient characteristics are shown in **Table 1**. Risk groups are based on WHO classification. All subjects signed informed consent forms. Sample acquisition was approved by COH Institutional Review Board in accordance with the Declaration of Helsinki. Mononuclear cells were isolated by Ficoll-Paque plus (Cytivia, Cat# 17-1440-03) centrifugation. $CD34^+$ cells selection was performed using immunomagnetic columns (Miltenyi Biotech, Cat# 130-046-701).

Orthotopic patient-derived AML xenograft model

Pretreated $CD34^+$ AML specimens (1×10^6 cells per mouse) were transplanted via tail vein injection into sub-lethally irradiated (180 cGy) 6-8-week-old female NSGS mice as described previously [24]. Mice were euthanized at 12 weeks post transplantation, and bone marrow content of femurs and spleen cells were assessed for long-term engraftment by labeling with APC anti-human CD45 antibody (Cat# 368512) and PE anti-human CD33 antibody (Cat# 366608) (BioLegend), followed by flow cytometry analysis. Mouse care and experimental procedures complied with established institutional guidance and approved protocols from the Institutional Animal Care and Use Committee at City of Hope National Medical Center.

Measurement of intracellular GTP by quantitative LC-MS/MS

AML cells were treated with 100 μM guanosine (Millipore Sigma, Cat# G6752) or 1 μM forodesine (Cayman Chemical, Item No. 30475) as indicated in RPMI 1640 medium supplemented with heat-inactivated dialyzed FBS (Cytiva, Cat# SH30079.03). Nucleotides were extracted using 100 μL ice-cold methanol/acetonitrile (50% V/V) containing stable isotopically labelled internal standards followed by three freeze-thaw cycles. Proteins were precipitated by centrifugation at 13,000 rpm for 15 min at

4°C; supernatants were then further diluted using 400 µL of water. The LC-MS/MS analysis of metabolite extract was performed using a Vanquish UHPLC coupled to a TSQ Altis triple quadrupole mass spectrometer (ThermoFisher, San Jose, CA). The separation was performed using a Hypercarb™ column (100 mm × 2.1 mm, 5 µm) (Thermo Fisher Scientific) with a 12 min gradient as previously descried [27]. The injection volume was 10 µL. Mass spectrometry analysis was performed using multiple reaction monitoring in negative ionization mode, with parameters as follows: spray voltage at 2600, sheath gas at 60, auxiliary gas at 15, sweep cone at 2, ion transfer tube temperature at 380°C and vaporization temperature at 350°C. The optimized collision energy and RF lens values for analytes are summarized in the table below.

Compound	Precursor (m/z)	Product (m/z)	Collision Energy (V)	RF Lens (V)
GTP	522	78.9	55	140
GTP	522	150	41.5	140
GTP	522	158.9	37.6	140
$^{13}C_{10}$,$^{15}N_5$-ATP	521	78.9	49.96	89
$^{13}C_{10}$,$^{15}N_5$-ATP	521	159	29.37	89
$^{13}C_{10}$,$^{15}N_5$-ATP	521	423	19.4	89

Both GTP and internal standard ($^{13}C_{10}$, $^{15}N_5$-ATP) were purchased from Sigma-Aldrich (St. Louis, MO). Stock and working solutions were prepared in LC-MS grade water. A ten-point calibration curve and quality controls at low, medium and high concentration were prepared in analyte-free matrix at 0.01 to 12 nmoles/1 × 10^6 cells. Analyte-free cell matrix was generated using charcoal activation [28]. Calibration curves showed excellent linearity (all correlation coefficient of >0.99) with accuracy and precision within 15%.

Metabolomic analysis and ^{15}N-glutamine labeling

U937 cells were cultured in RPMI 1640 medium supplemented with 10% heat-inactivated dialyzed FBS, 1% streptomycin/penicillin and 2 mM [amide-^{15}N] glutamine (Cat# NLM-557-1, Cambridge Isotope Laboratories) and treated with 100 µM guanosine for 12 hours. Metabolites were extracted with 80% methanol followed by centrifugation at 4°C. The supernatant was collected and evaporated to dryness on Vacufuge Plus (Eppendorf) at 30°C. Metabolites were resuspended in 50% acetonitrile and subjected to targeted metabolomic analysis on the UltiMate 3000 UPLC chromatography system coupled with a Thermo Scientific Q Exactive mass spectrometer. The chromatographic separation was achieved on a Luna 3u NH2 100A (150 × 2.0 mm) column (Phenomenex), and performed on a Vanquish Flex (Thermo Scientific) with 5 mM NH4AcO (pH 9.9, mobile phase A) and acetonitrile (mobile phase B) at a flow rate of 200 µl/min. The linear gradient from 15% A to 95% A over 18 min was followed by an isocratic step at 95% A for 9 min and re-equilibration. The Q Exactive mass spectrometer was run with polarity switching (+3.5 kV/-3.5 kV) in full scan mode with an m/z range of 70-975 and 70.000 resolution. TraceFinder 4.1 (Thermo Scientific) was used to quantify targeted metabolites by area under the curve (AUC) using accurate mass measurements (±3 ppm) and expected retention times. Relative abundances of metabolites were calculated by summing up the values of all isotopologues for a given metabolite. To plot the heatmap, the detection levels for all metabolites were further transformed by Z-score normalization.

GTP or MANT-GTP electroporation

Briefly, U937 cells were electroporated in Nucleofector™ solution buffer containing MANT-GTP (Abcam, Cat# ab146757) or GTP (Sigma-Aldrich, Cat# G8877) using Amaxa™ 4D-Nucleofector™ System (LONZA, Cat# V4XC-2024) according to the manufacturer's instructions. For MANT-GTP electroporation, cells were subject to flow cytometry analysis via 355 450_50 channel based on 7-AAD negative gate. For GTP electroporation, cells were washed with PBS and harvested for quantification of intracellular GTP, or continuously incubated in heat-inactivated media for 96 hours followed by flow cytometry analysis of surface markers.

Lentivirus production

Replication-incompetent lentiviruses were obtained as described previously [24]. Briefly, 293T cells were transiently transfected with pMD2.G, psPAX2 packaging plasmids as well as specific lentivectors by calcium-phosphate co-precipitation. Supernatants containing virus

particles were harvested, filtered, and concentrated using PEG-it (System Biosciences).

Generation of genetic knockout CRISPR-Cas9 cells

Oligonucleotides encoding for PNP gRNAs were CACCGAGATTATTGCAACTTGAGGT (fwd) and AAACACCTCAAGTTGCAATAATCTC (rev). Oligonucleotides encoding for HPRT1 gRNAs were CACCGCTCATGGACTAATTATGGAC (fwd) and AAACGTCCATAATTAGTCCATGAGC (rev). Oligonucleotides encoding for non-targeting control gRNAs were CACCGGATTCTAAAACGGATTACCA (fwd) and AAACTGGTAATCCGTTTTAGAATCC (rev). Oligos were annealed and inserted into BsmBI-cut lentiviral vector ipUSEPR, which contains RFP and puromycin as dual selection markers. After lentivirus production and titration, Cas9-expressing U937 cells were transduced at an estimated multiplicity of infection (MOI) of 1 in the presence of 8 μg/mL polybrene via spinoculation. Transduced bulk cells were selected with 2 μg/mL puromycin and subjected to single cell isolation by flow cytometry. Individual single-cell clones with disrupted gene expression were identified by western blot. Genomic DNA was prepared using QuickExtract™ DNA Extraction Solution (Lucigen, Cat# QE09050) according to manufacturer's protocol. Clones were then genotyped by sequencing of genomic DNA using the following primers: PNP- GAAGGGTGGCTGAGTAGATGG (fwd) and GCCTCCTTGGTTGTGTTCCA (rev); HPRT1- TGTAATGCTCTCATTGAAACAGC (fwd) and CTGGCTAGAGTTCCTTCTTCCA (rev).

Western blot

Cells were lysed in buffer containing 50 mM Tris (pH 7.4), 150 mM NaCl, 1 mM EDTA, 0.5% NP40, and 0.5% sodium deoxycholate, supplemented with protease and phosphatase inhibitors. Boiled lysates were resolved on 12% sodium dodecyl sulfate-polyacrylamide gel electrophoresis (SDS-PAGE) gels and transferred to nitrocellulose membranes (Bio-Rad). Proteins of interest were sequentially probed with primary and secondary antibodies. Horseradish peroxidase-conjugated secondary antibodies were from Jackson ImmunoResearch Laboratories (Westgrove, PA). Antibody detection was performed with SuperSignal™ West Pico or Femto kits (Thermo Fisher Scientific). Results were imaged by G: BOX Chemi XX6 gel doc systems (Syngene) and visualized using GeneSys image acquisition software (Syngene). All the antibodies were obtained from commercial sources. PNP antibody was from Genetex (Cat# GTX117364). HPRT1 antibody was from Proteintech (Cat# 15059-1-AP). β-actin antibody was from Santa Cruz Biotechnology (Cat# sc-69879).

Wight-Giemsa staining

Cytospins were prepared by diluting 200,000 cells in 100 μl PBS and spinning onto glass slides. Cells were fixed in absolute methanol, stained in Wright-Giemsa stain solution (Thermo Fisher Scientific, Cat# 9990710), and rinsed in pH 6.6 phosphate buffer. Images were acquired and analyzed under an INFINITY 2 microscope camera (Lumenera) and imaging software.

Statistics

Data were presented as mean ± SD as indicated. Two-tailed Student's t test, one-way ANOVA with multiple comparisons were performed as appropriate. $P<0.05$ was considered statistically significant.

Results

Guanosine treatment induces AML growth inhibition and differentiation

To examine the effects of exogenous supplementation of nucleotide triphosphates (NTPs) in AML, we exposed U937 cell line, which is widely used for studying monocyte/macrophage differentiation [15, 29], to a series of concentrations of ATP, UTP, CTP and GTP, respectively. Unexpectedly, GTP showed the most prominent growth-suppression with an IC_{50} of approximately 15 μM (**Figure 1A**). Notably, we performed the above assay in culture media supplemented with native FBS, which contains extracellular nucleotidases capable of degrading exogenous nucleotides [30]. Indeed, the growth inhibitory effect of GTP was almost fully diminished once U937 cells were cultured with heat-inactivated media (**Figure 1A**), where serum-derived enzymes were quenched. Furthermore, supplementation of individual ribonucleosides (adenosine, uridine, cytidine, and guanosine) recapitulated similar effects as their triphosphate counter-

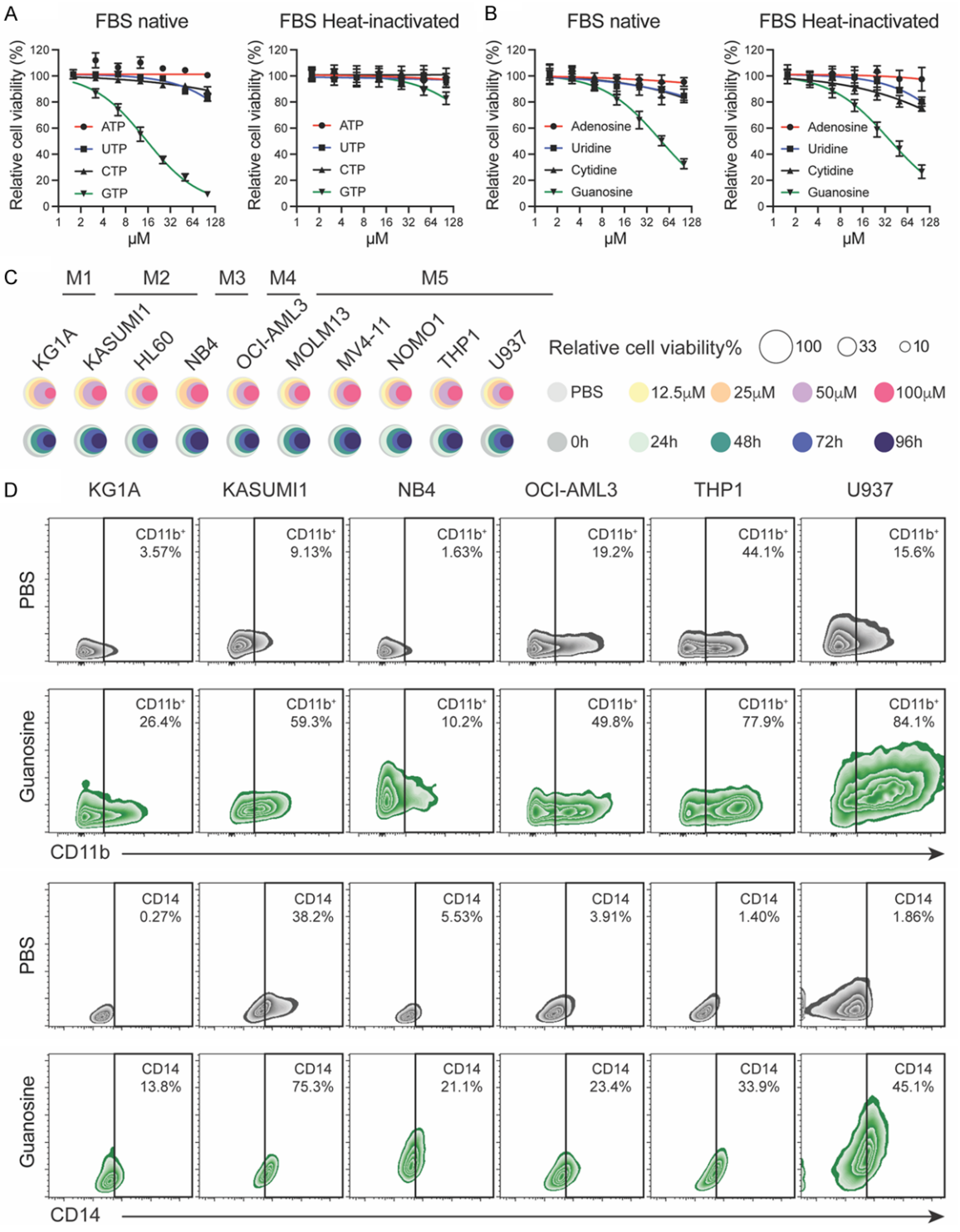

Figure 1. Guanosine treatment induces AML growth inhibition and differentiation. A. Relative cell viability of U937 cells treated with various doses of ribonucleoside 5'-triphosphates (ATP, UTP, CTP, GTP) respectively in culture media supplemented with native FBS (left) or heat-inactivated FBS (right). Data are presented as mean ± SD from triplicates. B. Relative cell viability of U937 cells treated with various doses of ribonucleosides (adenosine, uridine, cytidine, guanosine) respectively in culture media supplemented with native FBS (left) or heat-inactivated FBS (right). Data are presented as mean ± SD from triplicates. C. Dose- and time-dependent growth inhibition effects of guanosine on leukemia cell lines across different FAB subtypes. Cells were treated with different concentrations of guanosine for 96 hours (upper panel) or 100 μM guanosine for the indicated durations (lower panel). The colors denote different doses or timepoints and the diameter represents relative cell viability based on CellTiter Glo assay. D. CD11b and CD14 expression levels in indicated AML cell lines treated with 100 μM guanosine or PBS control for 96 hours. The percentages of $CD11b^+$ gates and $CD14^+$ gates are shown.

parts within native FBS-containing media, while these effects were not affected by heat inactivation (**Figure 1B**), indicating that guanosine acts as an essential intermediate for GTP-induced growth inhibition (Supplementary Figure 1A).

We further tested the effects of guanosine on other AML cell lines across various subtypes, including KG1A, KASUMI1, HL60, NB4, OCI-AML3, MOLM13, MV4-11, NOMO1 and THP1. Guanosine treatment inhibited cell proliferation in a time- and dose-dependent manner (**Figure 1C**), with IC_{50} ranging from 30 μM to 50 μM. Meanwhile, increased expression levels of myeloid surface markers CD11b and CD14 [31, 32] were also observed at varying degrees (**Figure 1D**). Morphological changes associated with myeloid differentiation were also evident in guanosine-treated cells (Supplementary Figure 1B), such as nuclear condensation and lobulation, decreased cytoplasmic basophilia [33]. We next treated U937 cells with guanosine or PBS control for 3 days and performed RNA sequencing. Differentially expressed gene analysis revealed 539 up-regulated genes ($P<0.05$, fold-change >1.5) and 467 down-regulated genes ($P<0.05$, fold-change <0.67) (Supplementary Figure 1C; Supplementary Table 1). Notably, there were many well-characterized myeloid differentiation genes being significantly up-regulated, including LYZ, S100A9, S100A8, NCF1, SPI1, EMR2, MAFB, CSF1R and EGR1 (Supplementary Figure 1C) [34-36]. Through GSEA analysis, gene sets indicating myeloid maturation were positively enriched in the guanosine-treated cells (**Figure 2A-C**). Conversely, genes defining proliferation and self-renewal potential were negatively enriched upon guanosine treatment, including SOX4 and SHMT2 (**Figure 2C**) [15, 37]. We further analyzed those 539 up-regulated genes by applying Ingenuity Pathway Analysis (IPA) to annotate their predicted biological significance [38, 39], and found these genes were closely linked to myeloid differentiation, inflammation (**Figure 2D**) or myeloid cell functions (Supplementary Figure 1D; Supplementary Table 2). These results suggest a differentiation-induction effect of guanosine on AML cells.

Guanosine treatment impairs leukemia cell growth in vivo

We next evaluated the effects of guanosine on leukemia initiation and progression by using U937 orthotopic xenograft model. Briefly, cells were first engineered with a luciferase/GFP expression cassette and then treated with guanosine or PBS control before injection into NSGS mice via tail vein. Mice injected with PBS-treated cells developed aggressive leukemia as evidenced by robust bioluminescence levels after two weeks (**Figure 3A**, **3B**) and succumbed to systemic disease shortly within three weeks (**Figure 3C**). In contrast, mice xenografted with guanosine-pretreated cells exhibited significantly delayed disease progression as evidenced by reduced leukemia burden (**Figure 3A**, **3B**) and prolonged survival (**Figure 3C**). We then extended our test to primary $CD34^+$ cells from AML specimens (**Table 1**). Specifically, treatment of primary AML cells with guanosine increased CD11b/CD14 expression levels (**Figure 3D**) and reduced their colony-formation capacities (**Figure 3E**). We further transplanted guanosine-pretreated primary AML cells into NSGS mice (**Figure 3F**). At 12 weeks after transplantation, mice receiving guanosine-treated primary AML cells showed markedly reduced engraftment of human $CD45^+/CD33^+$ cells in both bone marrow and spleen (**Figure 3G**, **3H**), indicating that guanosine compromised long-term repopulating capacity of AML stem/progenitor cells.

Guanosine promotes differentiation through intracellular GTP accumulation

Upon cellular uptake, guanosine is first degraded to guanine by PNP-mediated phosphorolysis. Guanine can be directly converted to GMP by phosphoribosyl transferase HPRT1, the major metabolic enzyme for GMP salvage synthesis [41]. Reciprocally, GMP can be hydrolyzed to guanosine by nucleotidase NT5C2 [42], thus constituting a closed circuit between anabolism and catabolism (**Figure 4A**). To test whether guanosine promotes differentiation by disrupting GTP homeostasis, we assessed total GTP levels in guanosine-treated AML cells. HPLC/MS analysis revealed a remarkable increase in intracellular GTP levels after guanosine treatment for 72 hours (**Figure 4B**). Targeted metabolomic analysis encompassing all purine metabolites showed significantly increased levels of guanine and its nucleotides (i.e., GMP, GDP, GTP) at 12 hours after guanosine treatment (**Figure 4C**), indicating GTP accumulation possibly due to salvage biosynthesis from exogenous guanosine. Accordingly,

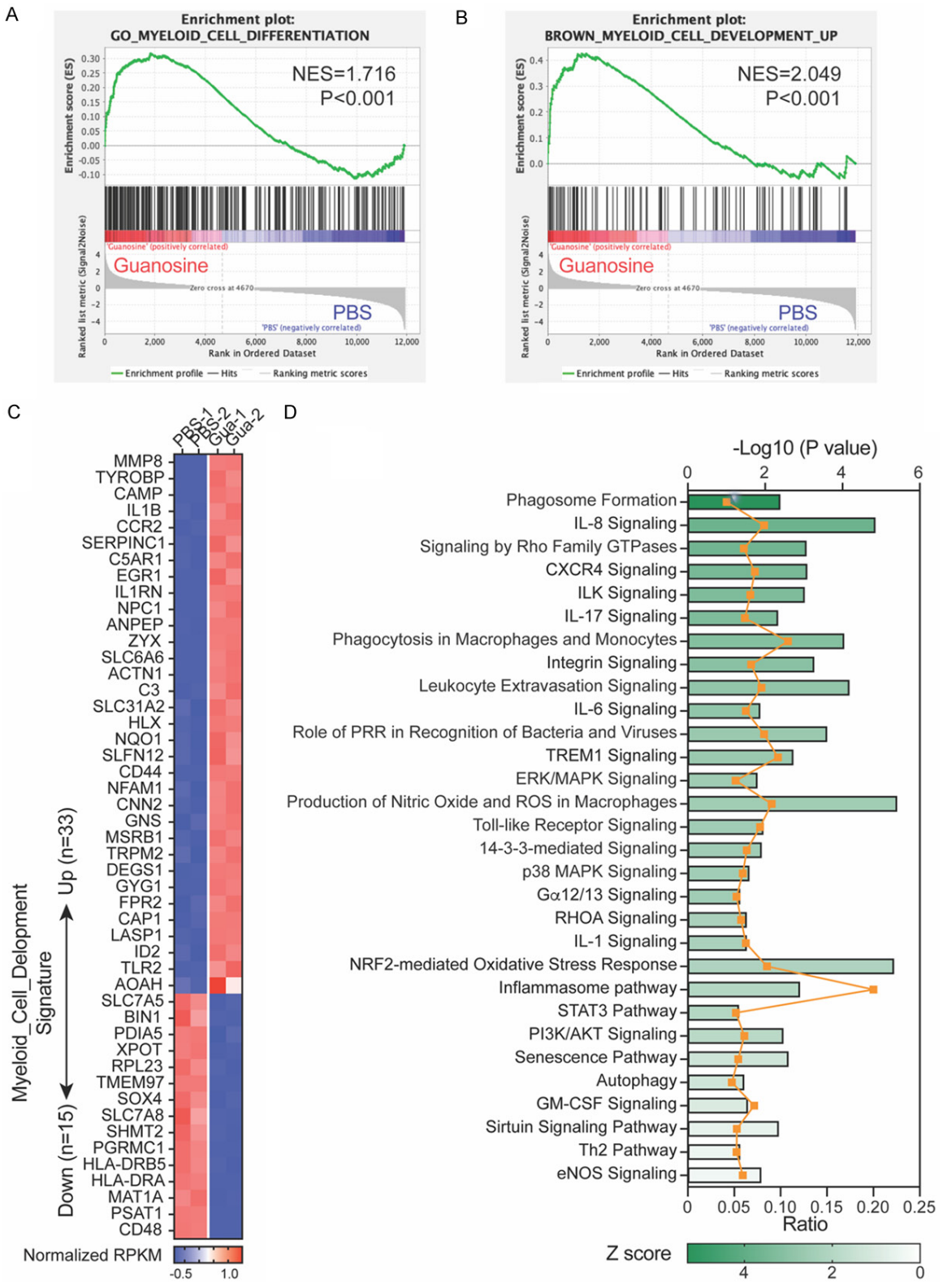

Figure 2. Guanosine induces gene expression program of myeloid differentiation. A. GSEA plot showing enrichment of GO_MYELOID_CELL_DIFFERENTIATION signature after guanosine treatment. The normalized enrichment scores (NES) and adjusted *P* values are indicated. B. GSEA plot showing enrichment of BROWN_MYELOID_CELL_DEVELOPMENT_UP signature after guanosine treatment. The normalized enrichment scores (NES) and adjusted *P* values are indicated. C. Heat map showing normalized expression of core enriched genes in guanosine-treated cells with

respect to the gene set "BROWN_MYELOID_CELL_DEVELOPMENT_UP", as well as core enriched genes in PBS controls with respect to the gene set "BROWN_MYELOID_CELL_DEVELOPMENT_DOWN". D. Pathway analysis of genes upregulated after guanosine treatment. Bars represent -Log_{10} *P* values for individual pathways as indicated on the top axis. Dots and curve represent ratio of upregulated genes overlapped with the pathway of interest as indicated on the bottom axis. Pathways are colored and ranked according to Z-score.

we further evaluated changes in purine nucleotide biosynthesis rates by measuring incorporation of ^{15}N originating from [amide-^{15}N] glutamine into purine rings [43, 44]. Apart from the nitrogen contained in phosphoribosylamine (PRA), glutamine donates one additional amide nitrogen to IMP/AMP and two additional amide nitrogens to GMP during de novo purine synthesis (Supplementary Figure 2A, 2B). Consistently, guanosine treatment resulted in a robust increase in fractions of unlabeled (M+0) guanine nucleotides, accompanied with a noticeable decrease in fractions of labeled (M+3) ones, the dominant newly synthesized form detected by mass spectrometry (**Figure 4D**). These data demonstrated that guanosine-induced GTP accumulation was sourced from active salvage synthesis.

We next asked whether direct introduction of GTP into cells in situ could mirror the effects of guanosine treatment. We developed an electroporation-based method as previously reported [45, 46]. To confirm electroporation efficiency, we first utilized a fluorescently labeled GTP analogue, MANT-GTP, and observed a percentage of 70% as MANT-GTP^+ population (Supplementary Figure 2C). We further electroporated U937 cells with GTP at gradually increasing doses and confirmed an increase in intracellular GTP levels comparable to those seen following guanosine treatment (**Figure 4E**). As expected, direct delivery of GTP into cells also induced differentiation as evidenced by CD11b upregulation (**Figure 4F**).

To corroborate the role of GTP accumulation in guanosine-mediated differentiation, we further treated U937 cells with guanosine in the presence of forodesine, a potent inhibitor of PNP [47]. Interestingly, while forodesine has minimal effects on the basal level of intracellular GTP, it efficiently blocked guanosine-induced GTP accumulation (**Figure 4G**), thereby reversing differentiation-induction (**Figure 4H**) and growth inhibition (**Figure 4I**). Collectively, we propose GTP accumulation as a functional metabolic event for exogenous guanosine to induce differentiation.

Genetic knockout of PNP or HPRT1 reverses guanosine-elicited differentiation

Our results noted above hinted an important role of PNP for guanosine-induced differentiation in AML. In fact, AML cells exhibit the most abundant expression of PNP compared with other common cancer cell lines (**Figure 5A**). We further depleted PNP in Cas9-expressing U937 cells using lentiviral sgRNA against PNP (**Figure 5B**, Supplementary Figure 3A). Consistent with utilization of forodesine, genetic knockout of PNP blocked the initial conversion of guanosine to guanine, thereby rescued guanosine-mediated GTP accumulation (**Figure 5C**) and differentiation (**Figure 5D**), as compared to U937 cells transduced with non-targeting sgRNA.

Given the critical role of PNP in facilitating guanosine-triggered salvage synthesis, we ask whether other gene in GTP salvage synthesis pathway is also involved. We first retrieved expression data from another public dataset in Depmap portal, including 44 AML cell lines. Correlation analysis ranked HPRT1 as the top positively correlated gene with PNP (**Figure 6A**, **6B**). We further depleted HPRT1 in Cas9-expressing U937 cells using lentiviral sgRNA directed against HPRT1 (**Figure 6C**, Supplementary Figure 3B). Similar to PNP, genetic knockout of HPRT1 reversed guanosine-mediated GTP accumulation (**Figure 6D**) and differentiation induction (**Figure 6E**). Taken together, these results suggest both PNP-mediated degradation and HPRT1-mediated salvage as indispensable prerequisites in exerting pro-differentiation and growth inhibitory effects of guanosine.

Discussion

GTP is the most prevalent guanine nucleotide in mammalian cells with its physiological cellular concentration varying in sub-millimolar range [48]. While intracellular GTP concentration dramatically changes in response to environment stress and pathological condition, whether it serves a metabolic cue for myeloid differentiation remains elusive. GTP depletion by targeted

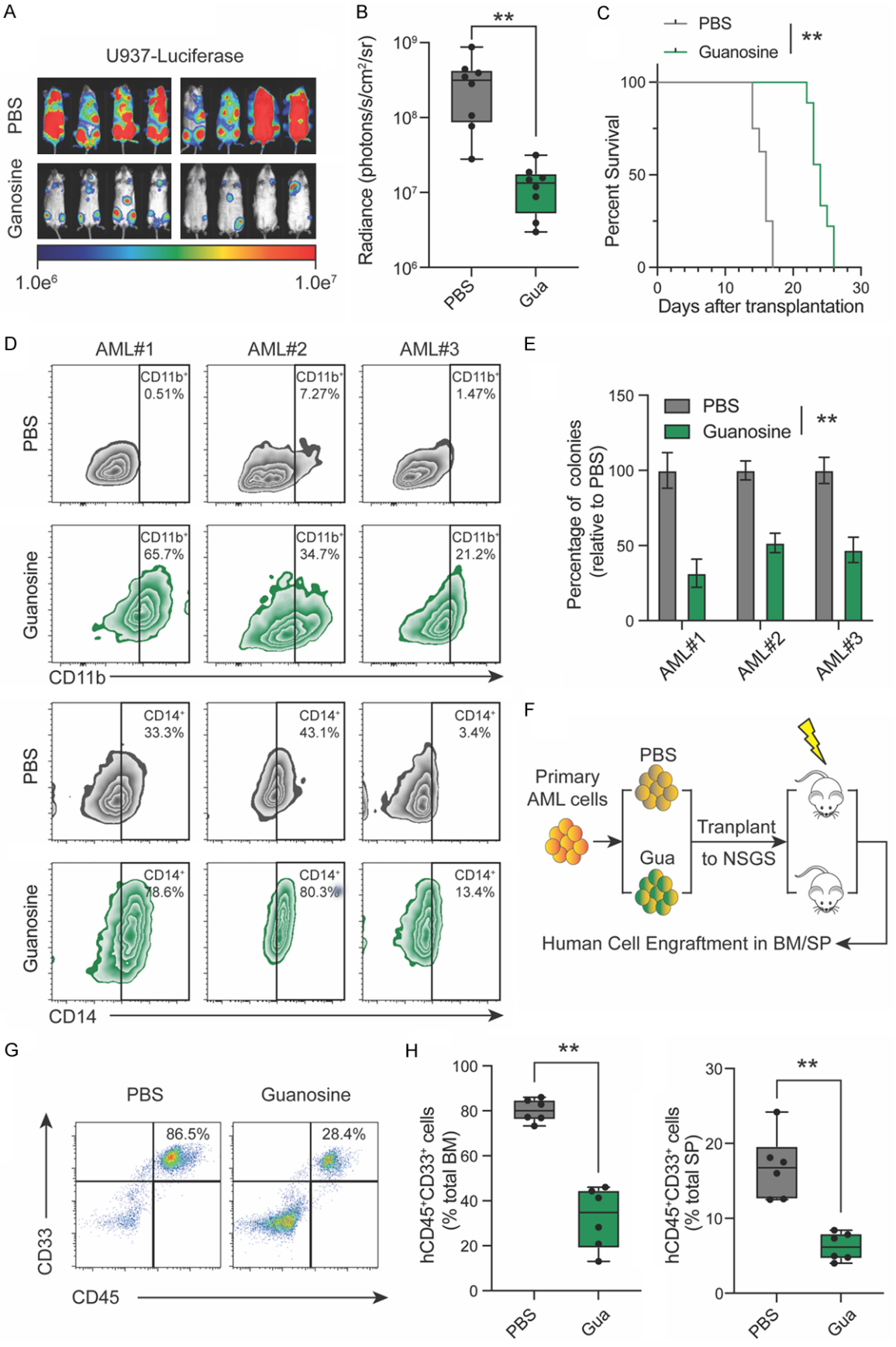
A
U937-Luciferase
PBS
Ganosine
1.0e6
1.0e7
B
**
Radiance (photons/s/cm²/sr)
PBS
Gua
C
PBS
Guanosine
**
Percent Survival
Days after transplantation
D
AML#1
AML#2
AML#3
CD11b⁺ 0.51%
CD11b⁺ 7.27%
CD11b⁺ 1.47%
CD11b⁺ 65.7%
CD11b⁺ 34.7%
CD11b⁺ 21.2%
CD11b
CD14⁺ 33.3%
CD14⁺ 43.1%
CD14⁺ 3.4%
CD14⁺ 78.6%
CD14⁺ 80.3%
CD14⁺ 13.4%
CD14
E
PBS
Guanosine
**
Percentage of colonies (relative to PBS)
F
Primary AML cells
PBS
Gua
Tranplant to NSGS
Human Cell Engraftment in BM/SP
G
PBS
Guanosine
86.5%
28.4%
CD33
CD45
H
**
hCD45⁺CD33⁺ cells (% total BM)
**
hCD45⁺CD33⁺ cells (% total SP)

Figure 3. Guanosine treatment impairs leukemia cell growth in vivo. (A-C) Luciferase-expressing U937 cells (0.5 × 10^6 cells per mouse) were first treated with 100 μM guanosine in vitro for 3 days before injection into sub-lethally irradiated NSGS mice. Leukemia cell engraftment was assessed by in vivo bioluminescence imaging (A). Quantitative radiances by bioluminescence on Day 14 post transplantation (B) are shown as box-whisker plots. **P<0.01 as assessed by student's t test. (C) Kaplan-Meier survival curves of mice. **P<0.01 as assessed by Mantel-Cox log-rank test. (D) CD11b and CD14 expression levels in indicated primary AML cells treated with 100 μM guanosine or PBS control for 96 hours. The percentages of $CD11b^+$ gates and $CD14^+$ gates are shown. (E) Colony formation in methylcellulose of 3 primary AML patient samples treated with 100 μM guanosine for two weeks. Data are normalized to PBS control for each sample and presented as mean ± SD. **P<0.01 as assessed by student's t test. (F) Schematic illustration of leukemic PDX model transplanted with AML cells from primary specimen AML #1 treated with 100 μM guanosine ex vivo for 3 days. Mice were sacrificed 12 weeks post transplantation and human cells were detected in bone marrow and spleen for assessment of long-term engraftment. (G) Representative CD45 and CD33 expression in bone marrow of NSGS xenografts. (H) Percentage of human $CD45^+/CD33^+$ cells in total bone marrow (left) and spleen (right). Data are shown as box-whisker plots. **P<0.01 as assessed by student's t test.

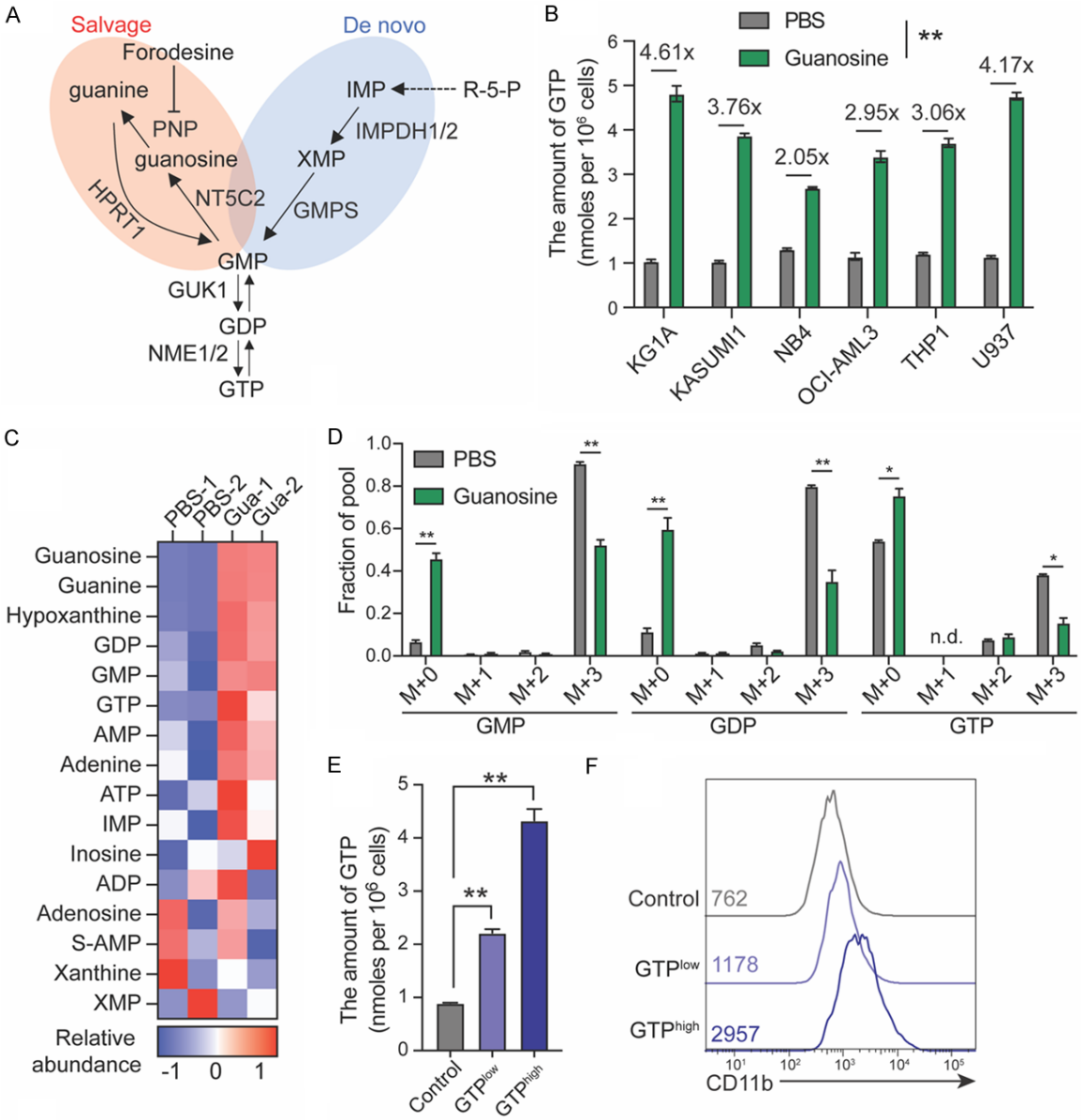

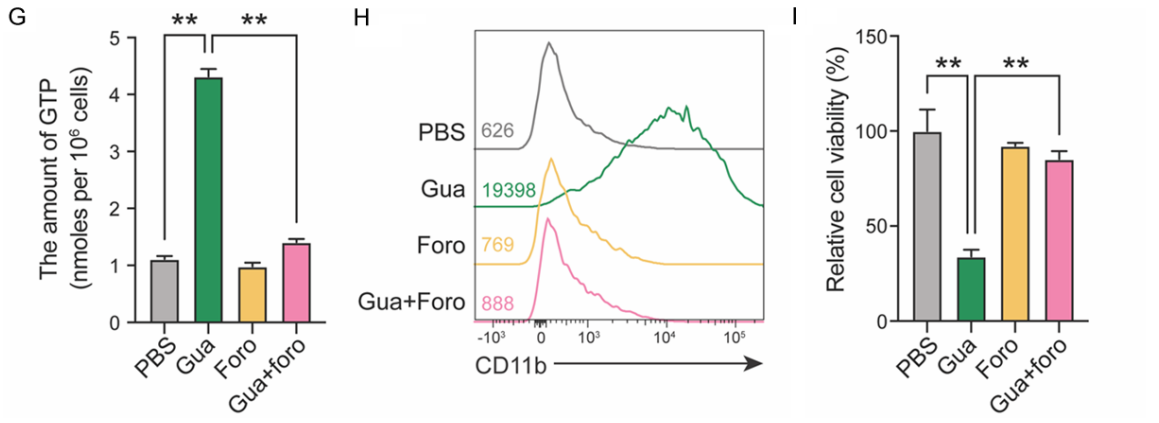

Figure 4. Guanosine promotes differentiation through intracellular GTP accumulation. (A) Overview of guanine nucleotide synthesis pathway. GMP can be either de novo synthesized starting from ribose 5'-phosphate, or directly salvaged from guanine by HPRT1. Meanwhile, GMP is hydrolyzed by NT5C2 to form guanosine, which is subsequently degraded to guanine by PNP. R-5-P, ribose 5'-phosphate; IMP, inosine monophosphate; XMP, xanthosine monophosphate; GMP, guanosine monophosphate; GDP, guanosine diphosphate; GTP, guanosine triphosphate; IMPDH, IMP dehydrogenase; GMPS, GMP synthetase; PNP, purine nucleoside phosphorylase; HPRT1, hypoxanthine phosphoribosyltransferase 1; NT5C2, 5'-nucleotidase, cytosolic II; GUK1, guanylate kinase 1; NME, NME/NM23 nucleoside diphosphate kinase. (B) AML cell lines were treated with 100 μM guanosine or PBS control for 72 hours. Intracellular GTP levels were quantified by HPLC/MS. For each cell line, data are presented as mean ± SD from duplicates. Numbers denote the fold change relative to controls. **P<0.01 as assessed by student's t test. (C) Heat map showing relative abundance of metabolites involved in purine metabolism. U937 cells were treated with 100 μM guanosine or PBS control for 12 hours and harvested for targeted HPLC-MS/MS. Z-score normalized intensities from duplicates are shown. (D) Fractional labeling of GMP, GDP and GTP in guanosine-treated or control U937 cells cultured in media containing [amide-^{15}N] glutamine for 12 hours. M+3 was the dominant labeled form. Data are presented as mean ± SD from duplicates. *P<0.05, **P<0.01 as assessed by student's t test. (E) U937 cells were electroporated with nucleofector solution containing different concentrations of GTP (GTP^{low} denotes 12.5 mM, GTP^{high} denotes 25 mM) or vehicle control. Cells were washed with PBS and collected at 4 hours after electroporation, and intracellular GTP levels were quantified by HPLC/MS. Data are presented as mean ± SD from duplicates. **P<0.01, one-way ANOVA with Sidak's multiple comparison test. (F) Representative CD11b expression levels of U937 cells electroporated with different concentrations of GTP as indicated above and incubated in heat-inactivated media for 96 hours. Mean fluorescence intensity (MFI) was indicated in histograms. (G) U937 cells were treated with PBS, guanosine (100 μM), forodesine (1 μM) or combination for 72 hours. Intracellular GTP levels were quantified by HPLC/MS. Data are presented as mean ± SD from duplicates. **P<0.01, one-way ANOVA with Sidak's multiple comparison test. (H, I) Representative CD11b expression levels (H) and relative cell viability (I) of U937 cells treated with PBS, guanosine (100 μM), forodesine (1 μM) or combination for 96 hours. For cell viability, data are presented as mean ± SD from triplicates. **P<0.01, one-way ANOVA with Sidak's multiple comparison test.

inhibition of its de novo biosynthesis shows detrimental effects on tumor cells including AML [49-52]. Herein, we demonstrate that a hyper-physiological level of intracellular GTP constitutes a key threshold toward terminal differentiation in AML, contrary to the prevailing view that nucleotide sufficiency exclusively promotes malignant proliferation in cancers. Our findings are consistent with a model raised from bacterial stress response [53, 54], where excess of GTP results in massive cell death. Moreover, GTP induces differentiation in human cells of different origins, including skeletal muscle cells [55], melanoma cells [56], and erythroleukemia cells [57]. These findings add a layer of complexity to this evolutionally conserved energy molecule.

We also characterized that the biological function of exogenous GTP was enacted by its corresponding nucleoside, guanosine. The discrepancy of growth inhibitory curves between FBS native media and FBS heat-inactivated media (**Figure 1A**) underscored the extracellular degradation of GTP to guanosine by serum-derived nucleotidases [30]. In line with previous reports [58], we also noted a lesser biological effect of guanosine compared to equimolar GTP (**Figure 1B**), probably due to the fact that exogenous guanosine is more prone to be irreversibly catabolized to guanine/xanthine/uric acid than guanosine derived from GTP [30].

We further dissected the role of salvage synthesis enzymes in guanosine-induced GTP

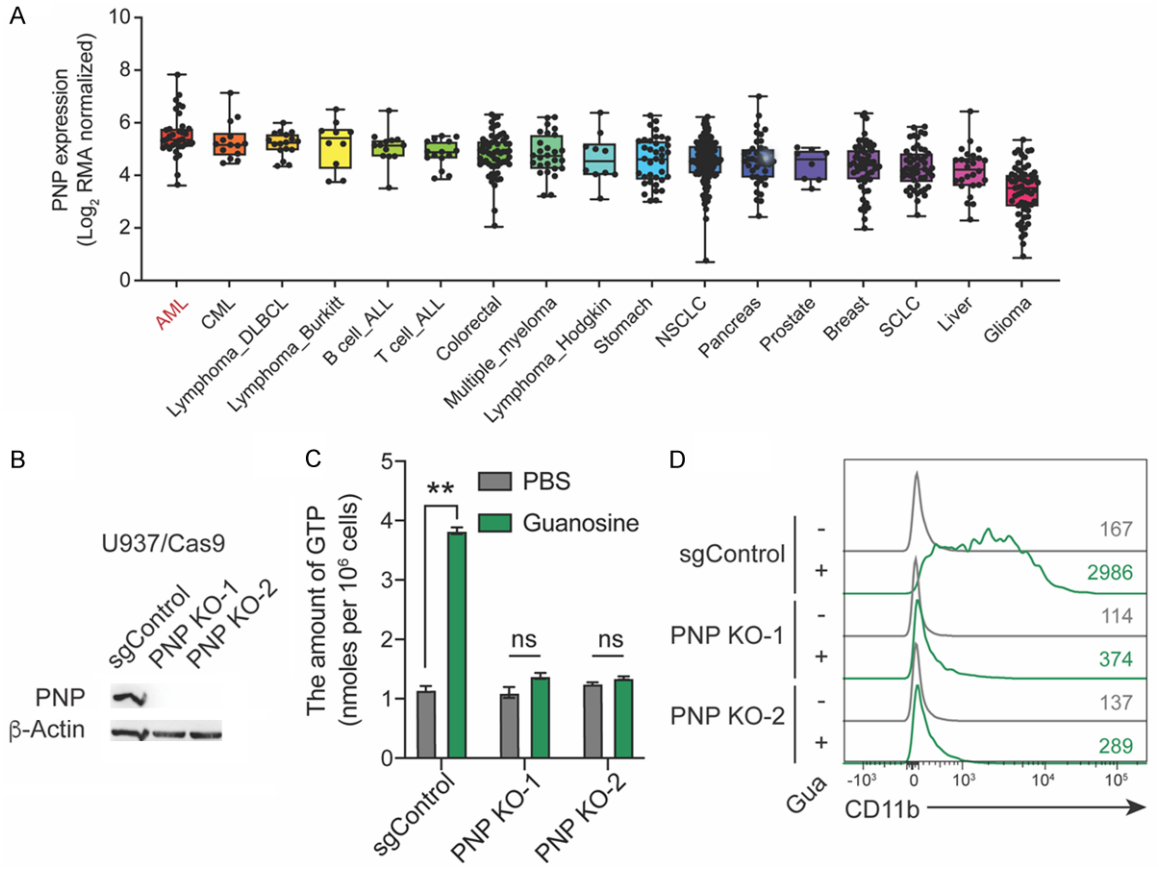

Figure 5. Genetic knockout of PNP reverses guanosine-elicited differentiation. A. Expression profiling for PNP across a panel of 604 cancer cell lines (including 35 AML cell lines) from CCLE. Data are presented as box-whisker plots where the mean, the minimum, and the maximum are indicated. B. Western blots of PNP in Cas9-expressing U937 cell clones transduced with lentiviral vectors expressing PNP-directed sgRNA (sgPNP). Bulk cells transduced with non-targeting sgRNA (sgControl) were served as the control. C. sgControl-transduced bulk cells and two validated sgPNP-transduced cell clones were treated with 100 μM guanosine or PBS control for 72 hours. Intracellular GTP levels were quantified by HPLC/MS. Data are presented as mean ± SD from duplicates. ns, not significant; $^{**}P<0.01$ as assessed by student's t test. D. Representative CD11b expression levels of U937-sgControl cells or U937 PNP KO cells treated with 100 μM guanosine or PBS control for 96 hours. MFI was indicated in histograms.

accumulation. Unlike other nucleosides that can be directly phosphorylated to synthesize their monophosphates, mammalian cells lack such a kinase to salvage guanosine [59]. Therefore, the primary metabolic fate of guanosine is PNP-catalyzed degradation. Indeed, metabolomic profiling in guanosine-treated cells showed accumulation of both guanine and hypoxanthine (**Figure 4C**), two metabolites downstream of PNP, generated from PNP-mediated phosphorolysis of guanosine and inosine, respectively. Moreover, our loss-of-function analysis established a crucial role of PNP in guanosine-induced differentiation (**Figures 4G-I**, **5B-D**). Nevertheless, it is yet to be answered how PNP functionally senses the dramatic surge of intracellular guanosine concentration arising from its physiological level [23]. It also warrants further investigation whether PNP could serve as a biomarker to predict response to guanosine-based therapeutic inventions in AML cells.

The mechanisms underlying differentiation induction by GTP overload remain unknown. The primary biological functions of GTP are nucleic acid synthesis, signal transduction and energy currency [43]. High levels of GTP support rRNA transcription and ribosome biogenesis [49, 60], which may lead to overinvestment in translation machinery at the expense of other essential products necessary for self-renewal [53]. Drastic dysregulation of GTP homeostasis may also affect GTP-responsive

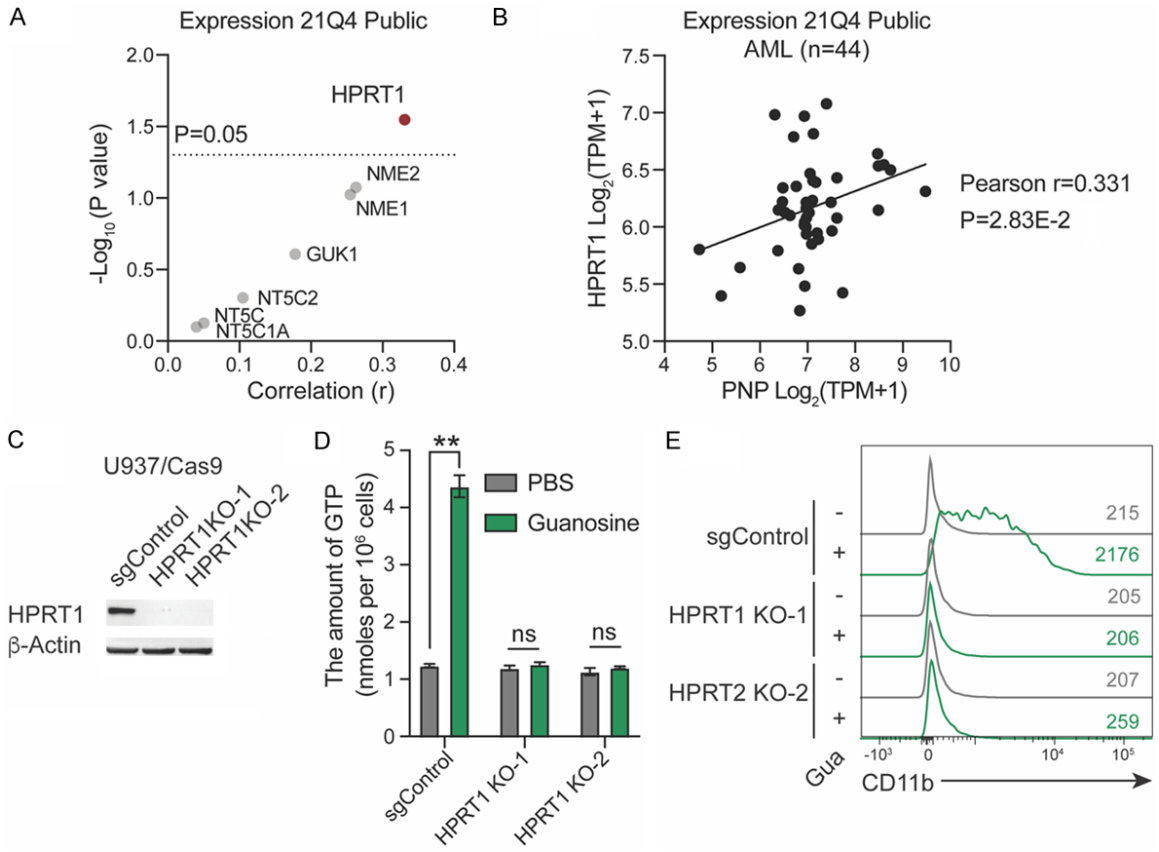

Figure 6. Guanosine-caused GTP accumulation depends on HPRT1-mediated salvage synthesis. (A) Pearson correlation coefficients of mRNA abundance between PNP and other transcripts of genes in guanine nucleotide salvage pathways from a panel of 44 AML cell lines. Dashed lines demarcate P=0.05 for linear regression. (B) Pearson correlation of PNP and HPRT1 expression as indicated in (A). (C) Western blots of HPRT1 in Cas9-expressing U937 cell clones transduced with lentiviral vectors expressing HPRT1-directed sgRNA (sgHPRT1). Bulk cells transduced with non-targeting sgRNA (sgControl) were served as the control. (D) sgControl-transduced bulk cells and two validated sgHPRT1-transduced cell clones were treated with 100 μM guanosine or PBS control for 72 hours. Intracellular GTP levels were quantified by HPLC/MS. Data are presented as mean ± SD from duplicates. ns, not significant; **P<0.01 as assessed by student's t test. (E) Representative CD11b expression levels of U937-sgControl cells or U937 HPRT1 KO cells treated with 100 μM guanosine or PBS control for 96 hours. MFI was indicated in histograms.

signaling involved in differentiation. Interestingly, our transcriptomic pathway analyses revealed guanosine treatment also significantly activated signaling of certain GTPases, including RAS/ERK pathway (**Figure 2D**), which has been functionally linked to myeloid differentiation [61-63] and hematopoietic stem cell exhaustion [64]. Furthermore, our isotope tracing data demonstrated that activation of guanosine-derived GTP salvage, in turn, resulted in a global decrease in fractions of newly synthesized adenine nucleotides (Supplementary Figure 2B), including those of labeled (M+2) ATP. Accordingly, guanosine-triggered inhibition of de novo ATP synthesis may dramatically alter the ratio of two energy currencies and poison ATP-utilizing proteins pivotal to leukemia maintenance.

Importantly, exogenous guanosine induces differentiation and impairs proliferation not only in AML cell lines across different subtypes, but also in primary AML cells carrying different cytogenetic/molecular alterations. Guanosine pretreatment also decreases the long-term engraftment of primary AML cells in immunodeficient xenograft models. Therefore, providing sufficient exogenous GTP or guanosine might be of clinical value to develop a new strategy for differentiation therapy in AML.

In conclusion, exogenous guanosine induces AML differentiation via PNP and HPRT1-de-

pendent salvage synthesis of excessive GTP. Our study provides justification for the advancement of guanosine or guanine nucleotides to clinical assessment in the treatment of AML patients.

Acknowledgements

We thank the COH Comprehensive Cancer Center, as well as patients and their physicians for providing primary specimens for this study. We thank Dr. Wei Chen from Integrative Genomics Core at COH for analyzing RNA sequencing data. We thank Dr. Khyatiben V. Pathak and Dr. Patrick Pirrotte from The Translational Genomics Research Institute for assistance with intracellular GTP measurements. We thank Dr. Xiyuan Lu and Dr. Stefano Tiziani from The University of Texas at Austin for assistance with isotope tracing and metabolomic analysis. This work was supported in part by Gehr Family Center for Leukemia Research support to L.L. We acknowledge the support of the Animal Resources Center, Analytical Cytometry Core at the COH Comprehensive Cancer Center, supported by the National Institutes of Health, National Cancer Institute under award number P30CA33572. The content is solely the responsibility of the authors and does not necessarily represent official views of the National Institutes of Health.

Disclosure of conflict of interest

None.

Address correspondence to: Dr. Xian Wang, Department of Medical Oncology, Sir Run Run Shaw Hospital, School of Medicine, Zhejiang University, 3 E. Qingchun Road, Hangzhou 310016, Zhejiang, China. Tel: +86-571-86006366; Fax: +86-571-86006145; E-mail: wangx118@zju.edu.cn; Dr. Ling Li, Department of Hematological Malignancies Translational Science, Gehr Family Center for Leukemia Research, Beckman Research Institute, City of Hope National Medical Center, 1500 E. Duarte Road, Duarte, CA 91010, USA. Tel: 626-218-2011; Fax: 626-301-8973; E-mail: lingli@coh.org

References

[1] Short NJ, Rytting ME and Cortes JE. Acute myeloid leukaemia. Lancet 2018; 392: 593-606.

[2] Talati C and Sweet K. Recently approved therapies in acute myeloid leukemia: a complex treatment landscape. Leuk Res 2018; 73: 58-66.

[3] Papaemmanuil E, Gerstung M, Bullinger L, Gaidzik VI, Paschka P, Roberts ND, Potter NE, Heuser M, Thol F, Bolli N, Gundem G, Van Loo P, Martincorena I, Ganly P, Mudie L, McLaren S, O'Meara S, Raine K, Jones DR, Teague JW, Butler AP, Greaves MF, Ganser A, Döhner K, Schlenk RF, Döhner H and Campbell PJ. Genomic classification and prognosis in acute myeloid leukemia. N Engl J Med 2016; 374: 2209-2221.

[4] de Thé H. Differentiation therapy revisited. Nat Rev Cancer 2018; 18: 117-127.

[5] Lewis AC and Kats LM. Non-genetic heterogeneity, altered cell fate and differentiation therapy. EMBO Mol Med 2021; 13: e12670.

[6] Madan V and Koeffler HP. Differentiation therapy of myeloid leukemia: four decades of development. Haematologica 2020; 106: 26-38.

[7] Losman JA, Looper RE, Koivunen P, Lee S, Schneider RK, McMahon C, Cowley GS, Root DE, Ebert BL and Kaelin WG Jr. (R)-2-hydroxyglutarate is sufficient to promote leukemogenesis and its effects are reversible. Science 2013; 339: 1621-1625.

[8] Wang F, Travins J, DeLaBarre B, Penard-Lacronique V, Schalm S, Hansen E, Straley K, Kernytsky A, Liu W, Gliser C, Yang H, Gross S, Artin E, Saada V, Mylonas E, Quivoron C, Popovici-Muller J, Saunders JO, Salituro FG, Yan S, Murray S, Wei W, Gao Y, Dang L, Dorsch M, Agresta S, Schenkein DP, Biller SA, Su SM, de Botton S and Yen KE. Targeted inhibition of mutant IDH2 in leukemia cells induces cellular differentiation. Science 2013; 340: 622-626.

[9] Roboz GJ, DiNardo CD, Stein EM, de Botton S, Mims AS, Prince GT, Altman JK, Arellano ML, Donnellan W, Erba HP, Mannis GN, Pollyea DA, Stein AS, Uy GL, Watts JM, Fathi AT, Kantarjian HM, Tallman MS, Choe S, Dai D, Fan B, Wang H, Zhang V, Yen KE, Kapsalis SM, Hickman D, Liu H, Agresta SV, Wu B, Attar EC and Stone RM. Ivosidenib induces deep durable remissions in patients with newly diagnosed IDH1-mutant acute myeloid leukemia. Blood 2020; 135: 463-471.

[10] Pollyea DA, Tallman MS, de Botton S, Kantarjian HM, Collins R, Stein AS, Frattini MG, Xu Q, Tosolini A, See WL, MacBeth KJ, Agresta SV, Attar EC, DiNardo CD and Stein EM. Enasidenib, an inhibitor of mutant IDH2 proteins, induces durable remissions in older patients with newly diagnosed acute myeloid leukemia. Leukemia 2019; 33: 2575-2584.

[11] Stein EM, DiNardo CD, Fathi AT, Mims AS, Pratz KW, Savona MR, Stein AS, Stone RM, Winer ES, Seet CS, Döhner H, Pollyea DA, McCloskey JK, Odenike O, Löwenberg B, Ossenkoppele

GJ, Patel PA, Roshal M, Frattini MG, Lersch F, Franovic A, Nabhan S, Fan B, Choe S, Wang H, Wu B, Hua L, Almon C, Cooper M, Kantarjian HM and Tallman MS. Ivosidenib or enasidenib combined with intensive chemotherapy in patients with newly diagnosed AML: a phase 1 study. Blood 2021; 137: 1792-1803.

[12] Rashkovan M and Ferrando A. Metabolic dependencies and vulnerabilities in leukemia. Genes Dev 2019; 33: 1460-1474.

[13] Tennant DA, Durán RV and Gottlieb E. Targeting metabolic transformation for cancer therapy. Nat Rev Cancer 2010; 10: 267-277.

[14] Dembitz V, Tomic B, Kodvanj I, Simon JA, Bedalov A and Visnjic D. The ribonucleoside AICAr induces differentiation of myeloid leukemia by activating the ATR/Chk1 via pyrimidine depletion. J Biol Chem 2019; 294: 15257-15270.

[15] Sykes DB, Kfoury YS, Mercier FE, Wawer MJ, Law JM, Haynes MK, Lewis TA, Schajnovitz A, Jain E, Lee D, Meyer H, Pierce KA, Tolliday NJ, Waller A, Ferrara SJ, Eheim AL, Stoeckigt D, Maxcy KL, Cobert JM, Bachand J, Szekely BA, Mukherjee S, Sklar LA, Kotz JD, Clish CB, Sadreyev RI, Clemons PA, Janzer A, Schreiber SL and Scadden DT. Inhibition of dihydroorotate dehydrogenase overcomes differentiation blockade in acute myeloid leukemia. Cell 2016; 167: 171-186, e115.

[16] Yamauchi T, Miyawaki K, Semba Y, Takahashi M, Izumi Y, Nogami J, Nakao F, Sugio T, Sasaki K, Pinello L, Bauer DE, Bamba T, Akashi K and Maeda T. Targeting leukemia-specific dependence on the de novo purine synthesis pathway. Leukemia 2021; [Epub ahead of print].

[17] Goyama S, Shikata S, Hayashi Y, Izawa Y, Schibler J, Iwamura H, Saito M, Kofuji S, Sumita K, Sasaki AT, Mulloy JC and Kitamura T. Inhibition of impdh as an effective treatment for MLL-fusion leukemia. Blood 2016; 128: 750.

[18] Di Marcantonio D, Martinez E, Kanefsky JS, Huhn JM, Gabbasov R, Gupta A, Krais JJ, Peri S, Tan Y, Skorski T, Dorrance A, Garzon R, Goldman AR, Tang HY, Johnson N and Sykes SM. ATF3 coordinates serine and nucleotide metabolism to drive cell cycle progression in acute myeloid leukemia. Mol Cell 2021; 81: 2752-2764, e2756.

[19] Bjelosevic S, Gruber E, Newbold A, Shembrey C, Devlin JR, Hogg SJ, Kats L, Todorovski I, Fan Z, Abrehart TC, Pomilio G, Wei A, Gregory GP, Vervoort SJ, Brown KK and Johnstone RW. Serine biosynthesis is a metabolic vulnerability in FLT3-ITD-driven acute myeloid leukemia. Cancer Discov 2021; 11: 1582-1599.

[20] Pikman Y, Puissant A, Alexe G, Furman A, Chen LM, Frumm SM, Ross L, Fenouille N, Bassil CF, Lewis CA, Ramos A, Gould J, Stone RM, DeAngelo DJ, Galinsky I, Clish CB, Kung AL, Hemann MT, Vander Heiden MG, Banerji V and Stegmaier K. Targeting MTHFD2 in acute myeloid leukemia. J Exp Med 2016; 213: 1285-1306.

[21] Siddiqui A and Ceppi P. A non-proliferative role of pyrimidine metabolism in cancer. Mol Metab 2020; 35: 100962.

[22] Chow SC, Kass GE and Orrenius S. Purines and their roles in apoptosis. Neuropharmacology 1997; 36: 1149-1156.

[23] Traut TW. Physiological concentrations of purines and pyrimidines. Mol Cell Biochem 1994; 140: 1-22.

[24] Sun J, He X, Zhu Y, Ding Z, Dong H, Feng Y, Du J, Wang H, Wu X, Zhang L, Yu X, Lin A, McDonald T, Zhao D, Wu H, Hua WK, Zhang B, Feng L, Tohyama K, Bhatia R, Oberdoerffer P, Chung YJ, Aplan PD, Boultwood J, Pellagatti A, Khaled S, Kortylewski M, Pichiorri F, Kuo YH, Carlesso N, Marcucci G, Jin H and Li L. SIRT1 activation disrupts maintenance of myelodysplastic syndrome stem and progenitor cells by restoring TET2 function. Cell Stem Cell 2018; 23: 355-369, e359.

[25] He X, Zhu Y, Lin YC, Li M, Du J, Dong H, Sun J, Zhu L, Wang H, Ding Z, Zhang L, Zhang L, Zhao D, Wang Z, Wu H, Zhang H, Jiang W, Xu Y, Jin J, Shen Y, Perry J, Zhao X, Zhang B, Liu S, Xue SL, Shen B, Chen CW, Chen J, Khaled S, Kuo YH, Marcucci G, Luo Y and Li L. PRMT1-mediated FLT3 arginine methylation promotes maintenance of FLT3-ITD(+) acute myeloid leukemia. Blood 2019; 134: 548-560.

[26] Li L, Osdal T, Ho Y, Chun S, McDonald T, Agarwal P, Lin A, Chu S, Qi J, Li L, Hsieh YT, Dos Santos C, Yuan H, Ha TQ, Popa M, Hovland R, Bruserud Ø, Gjertsen BT, Kuo YH, Chen W, Lain S, McCormack E and Bhatia R. SIRT1 activation by a c-MYC oncogenic network promotes the maintenance and drug resistance of human FLT3-ITD acute myeloid leukemia stem cells. Cell Stem Cell 2014; 15: 431-446.

[27] Zhu B, Wei H, Wang Q, Li F, Dai J, Yan C and Cheng Y. A simultaneously quantitative method to profiling twenty endogenous nucleosides and nucleotides in cancer cells using UHPLC-MS/MS. Talanta 2018; 179: 615-623.

[28] Thakare R, Chhonker YS, Gautam N, Alamoudi JA and Alnouti Y. Quantitative analysis of endogenous compounds. J Pharm Biomed Anal 2016; 128: 426-437.

[29] Wang L, Shao X, Zhong T, Wu Y, Xu A, Sun X, Gao H, Liu Y, Lan T, Tong Y, Tao X, Du W, Wang W, Chen Y, Li T, Meng X, Deng H, Yang B, He Q, Ying M and Rao Y. Discovery of a first-in-class CDK2 selective degrader for AML differentiation therapy. Nat Chem Biol 2021; 17: 567-575.

[30] Moosavi MA, Yazdanparast R and Lotfi A. GTP induces S-phase cell-cycle arrest and inhibits

DNA synthesis in K562 cells but not in normal human peripheral lymphocytes. J Biochem Mol Biol 2006; 39: 492-501.
[31] Theilgaard-Mönch K, Jacobsen LC, Borup R, Rasmussen T, Bjerregaard MD, Nielsen FC, Cowland JB and Borregaard N. The transcriptional program of terminal granulocytic differentiation. Blood 2005; 105: 1785-1796.
[32] Yazdanparast R, Moosavi MA, Mahdavi M and Lotfi A. Guanosine 5'-triphosphate induces differentiation-dependent apoptosis in human leukemia U937 and KG1 cells. Acta Pharmacol Sin 2006; 27: 1175-1184.
[33] Lainey E, Wolfromm A, Sukkurwala AQ, Micol J-B, Fenaux P, Galluzzi L, Kepp O and Kroemer G. EGFR inhibitors exacerbate differentiation and cell cycle arrest induced by retinoic acid and vitamin D3 in acute myeloid leukemia cells. Cell Cycle (Georgetown, Tex.) 2013; 12: 2978-2991.
[34] Behre G, Zhang P, Zhang DE and Tenen DG. Analysis of the modulation of transcriptional activity in myelopoiesis and leukemogenesis. Methods 1999; 17: 231-237.
[35] van Galen P, Hovestadt V, Wadsworth Ii MH, Hughes TK, Griffin GK, Battaglia S, Verga JA, Stephansky J, Pastika TJ, Lombardi Story J, Pinkus GS, Pozdnyakova O, Galinsky I, Stone RM, Graubert TA, Shalek AK, Aster JC, Lane AA and Bernstein BE. Single-cell RNA-seq reveals AML hierarchies relevant to disease progression and immunity. Cell 2019; 176: 1265-1281, e1224.
[36] Romine KA, Nechiporuk T, Bottomly D, Jeng S, McWeeney SK, Kaempf A, Corces MR, Majeti R and Tyner JW. Monocytic differentiation and AHR signaling as primary nodes of BET inhibitor response in acute myeloid leukemia. Blood Cancer Discov 2021; 2: 518.
[37] Pikman Y, Ocasio-Martinez N, Alexe G, Dimitrov B, Kitara S, Diehl FF, Robichaud AL, Conway AS, Ross L, Su A, Ling F, Qi J, Roti G, Lewis CA, Puissant A, Vander Heiden MG and Stegmaier K. Targeting serine hydroxymethyltransferases 1 and 2 for T-cell acute lymphoblastic leukemia therapy. Leukemia 2021; [Epub ahead of print].
[38] Franzini A, Pomicter AD, Yan D, Khorashad JS, Tantravahi SK, Than H, Ahmann JM, O'Hare T and Deininger MW. The transcriptome of CMML monocytes is highly inflammatory and reflects leukemia-specific and age-related alterations. Blood Adv 2019; 3: 2949-2961.
[39] Ye M, Zhang H, Yang H, Koche R, Staber PB, Cusan M, Levantini E, Welner RS, Bach CS, Zhang J, Krivtsov AV, Armstrong SA and Tenen DG. Hematopoietic differentiation is required for initiation of acute myeloid leukemia. Cell Stem Cell 2015; 17: 611-623.
[40] Pikman Y, Puissant A, Alexe G, Furman A, Chen LM, Frumm SM, Ross L, Fenouille N, Bassil CF, Lewis CA, Ramos A, Gould J, Stone RM, DeAngelo DJ, Galinsky I, Clish CB, Kung AL, Hemann MT, Vander Heiden MG, Banerji V and Stegmaier K. Targeting MTHFD2 in acute myeloid leukemia. J Exp Med 2016; 213: 1285-1306.
[41] Yin J, Ren W, Huang X, Deng J, Li T and Yin Y. Potential mechanisms connecting purine metabolism and cancer therapy. Front Immunol 2018; 9: 1697-1697.
[42] Oka J, Matsumoto A, Hosokawa Y and Inoue S. Molecular cloning of human cytosolic purine 5'-nucleotidase. Biochem Biophys Res Commun 1994; 205: 917-922.
[43] Huang F, Ni M, Chalishazar MD, Huffman KE, Kim J, Cai L, Shi X, Cai F, Zacharias LG, Ireland AS, Li K, Gu W, Kaushik AK, Liu X, Gazdar AF, Oliver TG, Minna JD, Hu Z and DeBerardinis RJ. Inosine monophosphate dehydrogenase dependence in a subset of small cell lung cancers. Cell Metab 2018; 28: 369-382, e365.
[44] Zhou W, Yao Y, Scott AJ, Wilder-Romans K, Dresser JJ, Werner CK, Sun H, Pratt D, Sajjakulnukit P, Zhao SG, Davis M, Nelson BS, Halbrook CJ, Zhang L, Gatto F, Umemura Y, Walker AK, Kachman M, Sarkaria JN, Xiong J, Morgan MA, Rehemtualla A, Castro MG, Lowenstein P, Chandrasekaran S, Lawrence TS, Lyssiotis CA and Wahl DR. Purine metabolism regulates DNA repair and therapy resistance in glioblastoma. Nat Commun 2020; 11: 3811.
[45] Finch RA, Chang DC and Chan PK. GTP gamma S restores nucleophosmin (NPM) localization to nucleoli of GTP-depleted HeLa cells. Mol Cell Biochem 1995; 146: 171-178.
[46] Brownell HL, Firth KL, Kawauchi K, Delovitch T and Raptis L. A novel technique for the study of ras activity: electroporation of [α-32P]GTP. DNA Cell Biol 1997; 16: 103-110.
[47] Davenne T, Klintman J, Sharma S, Rigby RE, Blest HTW, Cursi C, Bridgeman A, Dadonaite B, De Keersmaecker K, Hillmen P, Chabes A, Schuh A and Rehwinkel J. SAMHD1 limits the efficacy of forodesine in leukemia by protecting cells against the cytotoxicity of dGTP. Cell Rep 2020; 31: 107640.
[48] Sumita K, Lo YH, Takeuchi K, Senda M, Kofuji S, Ikeda Y, Terakawa J, Sasaki M, Yoshino H, Majd N, Zheng Y, Kahoud ER, Yokota T, Emerling BM, Asara JM, Ishida T, Locasale JW, Daikoku T, Anastasiou D, Senda T and Sasaki AT. The lipid kinase PI5P4Kβ is an intracellular GTP sensor for metabolism and tumorigenesis. Mol Cell 2016; 61: 187-198.
[49] Kofuji S, Hirayama A, Eberhardt AO, Kawaguchi R, Sugiura Y, Sampetrean O, Ikeda Y, Warren M, Sakamoto N, Kitahara S, Yoshino H, Yamashita D, Sumita K, Wolfe K, Lange L, Ikeda

S, Shimada H, Minami N, Malhotra A, Morioka S, Ban Y, Asano M, Flanary VL, Ramkissoon A, Chow LML, Kiyokawa J, Mashimo T, Lucey G, Mareninov S, Ozawa T, Onishi N, Okumura K, Terakawa J, Daikoku T, Wise-Draper T, Majd N, Kofuji K, Sasaki M, Mori M, Kanemura Y, Smith EP, Anastasiou D, Wakimoto H, Holland EC, Yong WH, Horbinski C, Nakano I, DeBerardinis RJ, Bachoo RM, Mischel PS, Yasui W, Suematsu M, Saya H, Soga T, Grummt I, Bierhoff H and Sasaki AT. IMP dehydrogenase-2 drives aberrant nucleolar activity and promotes tumorigenesis in glioblastoma. Nat Cell Biol 2019; 21: 1003-1014.

[50] Huang F, Huffman KE, Wang Z, Wang X, Li K, Cai F, Yang C, Cai L, Shih TS, Zacharias LG, Chung A, Yang Q, Chalishazar MD, Ireland AS, Stewart CA, Cargill K, Girard L, Liu Y, Ni M, Xu J, Wu X, Zhu H, Drapkin B, Byers LA, Oliver TG, Gazdar AF, Minna JD and DeBerardinis RJ. Guanosine triphosphate links MYC-dependent metabolic and ribosome programs in small-cell lung cancer. J Clin Invest 2021; 131: e139929.

[51] Chong YC, Toh TB, Chan Z, Lin QXX, Thng DKH, Hooi L, Ding Z, Shuen T, Toh HC, Dan YY, Bonney GK, Zhou L, Chow P, Wang Y, Benoukraf T, Chow EK and Han W. Targeted inhibition of purine metabolism is effective in suppressing hepatocellular carcinoma progression. Hepatol Commun 2020; 4: 1362-1381.

[52] Yang H, Fang Z, Wei Y, Bohannan ZS, Gañán-Gómez I, Pierola AA, Paradiso LJ, Iwamura H and Garcia-Manero G. Preclinical activity of FF-10501-01, a novel inosine-5'-monophosphate dehydrogenase inhibitor, in acute myeloid leukemia. Leuk Res 2017; 59: 85-92.

[53] Kriel A, Bittner AN, Kim SH, Liu K, Tehranchi AK, Zou WY, Rendon S, Chen R, Tu BP and Wang JD. Direct regulation of GTP homeostasis by (p)ppGpp: a critical component of viability and stress resistance. Mol Cell 2012; 48: 231-241.

[54] Petersen C. Inhibition of cellular growth by increased guanine nucleotide pools: characterization of an Escherichia coli mutant with a guanosine kinase that is insensitive to feedback inhibition by GTP. J Biol Chem 1999; 274: 5348-5356.

[55] Mancinelli R, Pietrangelo T, Burnstock G, Fanò G and Fulle S. Transcriptional profile of GTP-mediated differentiation of C2C12 skeletal muscle cells. Purinergic Signal 2012; 8: 207-221.

[56] Giotta GJ, Smith JR and Nicolson GL. Guanosine 5'-triphosphate inhibits growth and stimulates differentiated functions in B16 melanoma cells. Exp Cell Res 1978; 112: 385-393.

[57] Morceau F, Dupont C, Palissot V, Borde-Chiché P, Trentesaux C, Dicato M and Diederich M. GTP-mediated differentiation of the human K562 cell line: transient overexpression of GATA-1 and stabilization of the gamma-globin mRNA. Leukemia 2000; 14: 1589-1597.

[58] Schneider C, Wiendl H and Ogilvie A. Biphasic cytotoxic mechanism of extracellular ATP on U-937 human histiocytic leukemia cells: involvement of adenosine generation. Biochim Biophys Acta 2001; 1538: 190-205.

[59] Matsui H, Shimaoka M, Takenaka Y, Kawasaki H and Kurahashi O. gsk disruption leads to guanosine accumulation in Escherichia coli. Biosci Biotechnol Biochem 2001; 65: 1230-1235.

[60] Huang F, Huffman KE, Wang Z, Wang X, Li K, Cai F, Yang C, Cai L, Shih TS, Zacharias LG, Chung A, Yang Q, Chalishazar MD, Ireland AS, Stewart CA, Cargill K, Girard L, Liu Y, Ni M, Xu J, Wu X, Zhu H, Drapkin B, Byers LA, Oliver TG, Gazdar AF, Minna JD and DeBerardinis RJ. Guanosine triphosphate links MYC-dependent metabolic and ribosome programs in small-cell lung cancer. J Clin Invest 2021; 131: e139929.

[61] Yokoyama N, Kim YJ, Hirabayashi Y, Tabe Y, Takamori K, Ogawa H and Iwabuchi K. Kras promotes myeloid differentiation through Wnt/β-catenin signaling. FASEB Bioadv 2019; 1: 435-449.

[62] Pei S, Pollyea DA, Gustafson A, Stevens BM, Minhajuddin M, Fu R, Riemondy KA, Gillen AE, Sheridan RM, Kim J, Costello JC, Amaya ML, Inguva A, Winters A, Ye H, Krug A, Jones CL, Adane B, Khan N, Ponder J, Schowinsky J, Abbott D, Hammes A, Myers JR, Ashton JM, Nemkov T, D'Alessandro A, Gutman JA, Ramsey HE, Savona MR, Smith CA and Jordan CT. Monocytic subclones confer resistance to venetoclax-based therapy in patients with acute myeloid leukemia. Cancer Discov 2020; 10: 536-551.

[63] Brendel C, Teichler S, Millahn A, Stiewe T, Krause M, Stabla K, Ross P, Huynh M, Illmer T, Mernberger M, Barckhausen C and Neubauer A. Oncogenic NRAS primes primary acute myeloid leukemia cells for differentiation. PLoS One 2015; 10: e0123181.

[64] Baumgartner C, Toifl S, Farlik M, Halbritter F, Scheicher R, Fischer I, Sexl V, Bock C and Baccarini M. An ERK-dependent feedback mechanism prevents hematopoietic stem cell exhaustion. Cell Stem Cell 2018; 22: 879-892, e876.

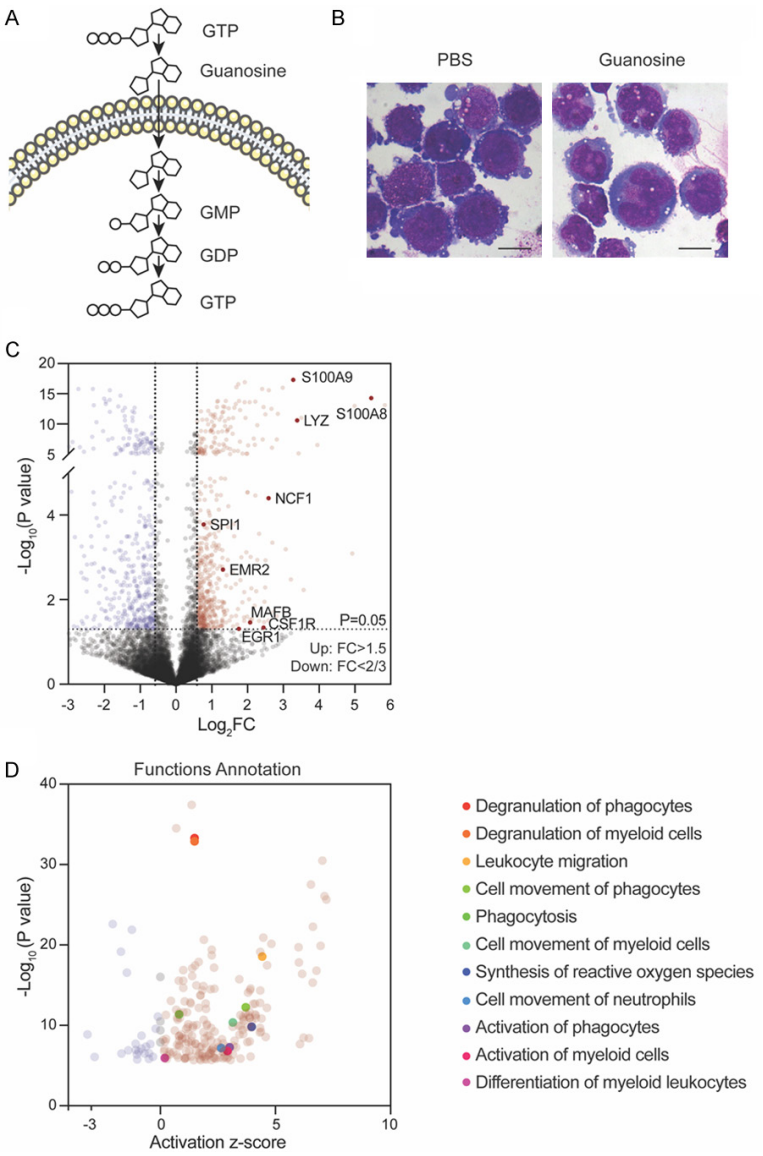

Supplemental Figure 1. Guanosine induces AML differentiation. (Related to **Figures 1**, **2**) A. The metabolic trajectory of exogenous GTP. GTP is not membrane permeable so that it is first degraded to guanosine by serum-derived nucleotidase before entering cells for sequential phosphorylation. B. Representative images of U937 cells treated with 100 μM guanosine or PBS control for 96 hours by Wright-Giemsa staining. Scale bar, 10 μm. C. Volcano plot showing differentially expressed genes in guanosine-treated U937 cells versus PBS-treated controls. Horizontal dashed line indicates P=0.05 as statistical cutoff. Vertical dashed lines indicate FC=1.5 or FC=0.67 as expression cutoff for up-regulated genes (in red) and down-regulated genes (in blue), respectively. Highlighted are exemplary genes reported to be up-regulated during myeloid differentiation. D. Functional annotation of genes upregulated after guanosine treatment analyzed by IPA. Highlighted are functional terms associated with myeloid differentiation showing positive z score and significant *P* value (P<0.01).

Supplementary Table 2. Diseases or functions annotations of 539 up-regulated genes in guanosine-treated U937 cells versus PBS controls retrieved by IPA (Related to Supplementary Figure 1)

Categories	Diseases or Functions Annotation	*P*-value	Activation z-score
Cancer, Gastrointestinal Disease, Organismal Injury and Abnormalities	Digestive organ tumor	6.62E-13	1.671
Cancer, Hematological Disease, Organismal Injury and Abnormalities	Hematopoietic neoplasm	7.98E-18	1.387
Cancer, Neurological Disease, Organismal Injury and Abnormalities	Central nervous system solid tumor	3.20E-11	0.000
	Glioma	4.12E-10	0.000
Cancer, Organismal Injury and Abnormalities	Invasion of tissue	1.37E-09	3.440
	Cancer	1.80E-16	3.429
	Malignant solid tumor	2.77E-15	2.350
	Nonhematologic malignant neoplasm	6.36E-18	2.333
	Epithelial neoplasm	3.97E-20	2.236
	Carcinoma	1.94E-19	2.236
	Solid tumor	3.18E-15	2.177
	Cancer of cells	8.95E-13	1.982
	Advanced malignant tumor	1.87E-13	1.969
	Tumorigenesis of tissue	2.20E-21	1.890
	Extracranial solid tumor	4.37E-15	1.824
	Invasive tumor	1.78E-14	1.741
	Metastasis	1.81E-14	1.741
	Non-melanoma solid tumor	1.29E-18	1.667
	Neoplasia of cells	1.01E-15	1.568
	Non-hematological solid tumor	3.46E-18	1.508
	Extra-pancreatic malignant tumor	7.24E-17	1.387
	Extra-adrenal retroperitoneal tumor	1.21E-08	1.219
	Abdominal neoplasm	1.33E-17	1.000
	Intraabdominal organ tumor	2.69E-16	1.000
	Abdominal cancer	2.15E-15	1.000
	Genitourinary tumor	2.28E-12	1.000
	Malignant genitourinary solid tumor	2.59E-12	0.816
	Malignant neoplasm of retroperitoneum	7.75E-09	0.816
	Formation of solid tumor	9.19E-17	0.000
Cancer, Organismal Injury and Abnormalities, Renal and Urological Disease	Renal cancer	2.03E-09	0.816
	Renal tumor	2.25E-09	0.816
	Urinary tract cancer	2.96E-08	0.816
	Urinary tract tumor	4.39E-08	0.816
Cardiovascular System Development and Function, Cell-To-Cell Signaling and Interaction	Adhesion of endothelial cells	1.21E-07	2.767
	Binding of endothelial cells	6.04E-08	2.299
Cardiovascular System Development and Function, Cellular Development, Cellular Function and Maintenance, Cellular Growth and Proliferation, Organismal Development, Tissue Development	Endothelial cell development	2.29E-07	2.170
Cardiovascular System Development and Function, Cellular Movement	Cell movement of endothelial cells	5.20E-08	3.291
	Migration of endothelial cells	9.12E-07	2.945
	Movement of vascular endothelial cells	1.41E-06	2.413
Cardiovascular System Development and Function, Organismal Development	Angiogenesis	6.40E-13	4.626
	Vasculogenesis	5.34E-12	3.481
Cell Cycle	Interaction of DNA	8.84E-11	1.592
	Interphase	2.53E-10	-0.198
	Interphase of tumor cell lines	7.42E-08	-0.817
Cell Cycle, Gene Expression	Binding of DNA	1.03E-10	1.430

Cell Death and Survival	Cell viability of tumor cell lines	3.91E-17	6.159
	Cell viability	1.48E-18	6.025
	Cell survival	1.94E-20	6.007
	Cell viability of breast cancer cell lines	5.79E-10	4.373
	Cell death of immune cells	4.38E-09	1.087
	Cell death of blood cells	3.36E-09	0.945
	Cell death of leukemia cell lines	1.30E-09	0.895
	Cell death of neutrophils	3.60E-07	0.443
	Cell death of phagocytes	6.05E-07	0.282
	Cell death of granulocytes	1.05E-08	0.213
	Apoptosis of leukemia cell lines	8.82E-08	0.187
	Cell death of myeloid cells	2.05E-08	-0.431
	Apoptosis of prostate cancer cell lines	2.87E-07	-0.485
	Necrosis of prostate cancer cell lines	4.33E-08	-0.621
	Apoptosis of phagocytes	3.19E-07	-0.686
	Cell death of cervical cancer cell lines	1.89E-09	-0.815
	Apoptosis of leukocytes	1.71E-07	-0.941
	Apoptosis of neutrophils	4.01E-07	-1.019
	Apoptosis of blood cells	1.11E-07	-1.066
	Apoptosis of granulocytes	1.91E-08	-1.074
	Necrosis	1.28E-22	-1.234
	Apoptosis of myeloid cells	1.28E-07	-1.388
	Apoptosis of tumor cell lines	2.68E-17	-1.456
	Cell death of carcinoma cell lines	3.17E-07	-1.683
	Cell death of tumor cell lines	6.68E-20	-1.706
	Apoptosis	2.41E-23	-2.067
	Apoptosis of breast cancer cell lines	8.48E-07	-2.854
	Cell death of breast cancer cell lines	1.30E-09	-3.161
Cell Death and Survival, Organismal Injury and Abnormalities	Necrosis of epithelial tissue	1.46E-06	-0.493
Cell Morphology, Cellular Movement	Cell spreading	3.68E-07	2.135
	Cell spreading of tumor cell lines	2.10E-06	1.445
Cell Morphology, Tissue Development	Tubulation of cells	2.03E-06	3.051
Cell Signaling, Cellular Function and Maintenance, Molecular Transport, Vitamin and Mineral Metabolism	Flux of Ca^{2+}	1.72E-08	2.733
Cell-To-Cell Signaling and Interaction	Binding of tumor cell lines	4.55E-15	4.339
	Binding of blood cells	4.21E-12	4.119
	Adhesion of blood cells	1.15E-11	3.880
	Activation of cells	5.66E-12	3.832
	Adhesion of tumor cell lines	8.47E-15	3.809
	Binding of lymphoid cells	1.48E-11	3.622
	Binding of leukemia cell lines	2.18E-07	2.972
	Adhesion of leukemia cell lines	8.39E-07	2.796
	Binding of melanoma cell lines	1.17E-06	2.733
	Response of endothelial cells	4.70E-08	1.998
	Interaction of lymphoma cell lines	7.94E-07	1.954
	Attachment of cells	6.86E-10	1.874
	Response of leukemia cell lines	5.04E-08	1.706
	Response of vascular cells	3.06E-07	1.706
	Attachment of tumor cell lines	1.42E-06	1.706
	Aggregation of cells	1.13E-06	1.066
	Response of tumor cell lines	2.65E-16	0.799
	Binding of myeloid cells	1.02E-06	0.780
	Communication of cells	2.03E-07	0.401
Cell-To-Cell Signaling and Interaction, Cellular Function and Maintenance, Hematological System Development and Function, Inflammatory Response	Phagocytosis of red blood cells	1.27E-08	0.000
Cell-To-Cell Signaling and Interaction, Cellular Function and Maintenance, Inflammatory Response	Phagocytosis of cells	1.15E-12	0.694
	Phagocytosis of blood cells	2.24E-07	0.554
	Phagocytosis of tumor cell lines	8.05E-12	-0.111

Cell-To-Cell Signaling and Interaction, Hematological System Development and Function	Binding of leukocytes	1.98E-13	4.115
	Interaction of lymphocytes	2.45E-11	3.621
	Binding of lymphocytes	1.11E-10	3.493
	Interaction of T lymphocytes	4.30E-08	2.902
	Binding of T lymphocytes	1.86E-07	2.739
	Activation of blood cells	1.86E-09	2.052
Cell-To-Cell Signaling and Interaction, Hematological System Development and Function, Immune Cell Trafficking	Adhesion of immune cells	2.07E-12	3.875
	Adhesion of lymphocytes	7.76E-09	3.225
Cell-To-Cell Signaling and Interaction, Hematological System Development and Function, Immune Cell Trafficking, Inflammatory Response	Activation of leukocytes	8.46E-08	2.257
Cell-To-Cell Signaling and Interaction, Inflammatory Response	Immune response of leukocytes	2.10E-06	1.750
	Immune response of tumor cell lines	8.62E-14	0.462
Cellular Assembly and Organization, Cellular Function and Maintenance	Organization of cytoskeleton	6.88E-11	2.027
	Organization of cytoplasm	1.04E-10	2.027
	Microtubule dynamics	5.13E-07	1.674
Cellular Compromise, Inflammatory Response	Degranulation of cells	3.65E-38	1.361
	Degranulation of leukocytes	3.02E-35	0.692
Cellular Development	Differentiation of tumor cell lines	1.04E-06	2.320
Cellular Development, Cellular Growth and Proliferation	Cell proliferation of tumor cell lines	7.28E-21	4.826
	Proliferation of prostate cancer cell lines	1.23E-06	2.891
	Cell proliferation of breast cancer cell lines	2.04E-11	1.881
	Development of tumor cell lines	8.92E-09	1.354
	Proliferation of blood cells	1.94E-13	1.322
	Proliferation of leukemia cell lines	1.01E-06	1.138
	Colony formation of breast cancer cell lines	1.72E-07	1.123
	Colony formation of tumor cell lines	1.89E-08	1.103
	Colony formation of cells	2.54E-08	0.735
	Colony formation of prostate cancer cell lines	7.76E-07	-0.321
Cellular Development, Cellular Growth and Proliferation, Hematological System Development and Function, Hematopoiesis, Lymphoid Tissue Structure and Development, Tissue Development	Myelopoiesis of leukocytes	1.64E-07	0.166
Cellular Development, Cellular Growth and Proliferation, Hematological System Development and Function, Humoral Immune Response, Lymphoid Tissue Structure and Development	Proliferation of B lymphocytes	2.97E-07	2.201
Cellular Development, Cellular Growth and Proliferation, Hematological System Development and Function, Lymphoid Tissue Structure and Development	Proliferation of immune cells	1.30E-13	1.301
	Proliferation of mononuclear leukocytes	2.27E-12	1.159
	Proliferation of lymphocytes	1.16E-11	0.735
	Cell proliferation of T lymphocytes	6.51E-09	0.118
Cellular Function and Maintenance	Endocytosis	1.91E-08	1.523
	Engulfment of cells	1.76E-10	1.417
	Endocytosis by eukaryotic cells	2.65E-10	1.125
	Engulfment of blood cells	4.83E-09	0.952
	Internalization of cells	1.18E-11	0.846
	Engulfment of tumor cell lines	4.77E-09	0.251
Cellular Growth and Proliferation	Proliferation of vascular cells	3.22E-07	1.825
	Colony formation	4.22E-10	0.634
Cellular Growth and Proliferation, Lymphoid Tissue Structure and Development	Proliferation of lymphatic system cells	1.88E-11	0.753
Cellular Growth and Proliferation, Tissue Development	Proliferation of epithelial cells	6.82E-07	1.841

Cellular Movement	Migration of cells	8.52E-27	7.137
	Cell movement	3.09E-31	7.042
	Invasion of cells	1.23E-20	6.961
	Invasion of tumor cell lines	1.55E-17	6.787
	Migration of tumor cell lines	5.35E-23	6.629
	Cell movement of tumor cell lines	3.05E-28	6.540
	Homing of cells	1.19E-21	4.474
	Chemotaxis	7.12E-20	4.340
	Migration of breast cancer cell lines	2.25E-13	4.030
	Invasion of prostate cancer cell lines	2.53E-15	3.925
	Invasion of carcinoma cell lines	7.37E-07	3.921
	Cell movement of breast cancer cell lines	4.34E-15	3.899
	Invasion of breast cancer cell lines	1.21E-08	3.780
	Cell movement of leukemia cell lines	1.22E-09	3.599
	Cell movement of carcinoma cell lines	3.71E-10	3.581
	Cell movement of lung cancer cell lines	1.49E-10	3.140
	Homing of tumor cell lines	9.89E-08	2.895
	Chemotaxis of tumor cell lines	2.02E-07	2.709
	Chemotaxis of myeloid cells	5.25E-09	2.676
	Cell movement of prostate cancer cell lines	1.04E-06	2.562
	Cell movement of cervical cancer cell lines	4.83E-08	2.536
	Migration of vascular cells	1.32E-08	2.482
	Migration of prostate cancer cell lines	1.15E-06	2.355
	Chemotaxis of carcinoma cell lines	2.03E-06	2.216
	Transmigration of cells	1.19E-07	2.215
	Invasion by eye cell lines	1.72E-06	2.000
Cellular Movement, Hematological System Development and Function	Cell movement of hematopoietic cells	2.07E-09	2.138
	Cell movement of hematopoietic progenitor cells	1.65E-08	1.912
	Migration of hematopoietic progenitor cells	7.52E-07	1.342
Cellular Movement, Hematological System Development and Function, Immune Cell Trafficking	Cell movement of leukocytes	3.34E-18	4.638
	Cell movement of mononuclear leukocytes	1.36E-11	4.394
	Migration of mononuclear leukocytes	1.91E-10	3.952
	Cell movement of lymphocytes	1.06E-11	3.884
	Lymphocyte migration	1.51E-10	3.771
	Cell movement of antigen presenting cells	2.08E-10	2.207
	Cell movement of granulocytes	4.15E-09	1.921
	Migration of antigen presenting cells	1.26E-06	1.081
Cellular Movement, Hematological System Development and Function, Immune Cell Trafficking, Inflammatory Response	Chemotaxis of leukocytes	1.13E-10	3.404
	Chemotaxis of phagocytes	3.45E-08	3.176
	Chemotaxis of neutrophils	5.71E-08	2.608
	Chemotaxis of granulocytes	7.25E-09	2.213
	Migration of phagocytes	1.89E-08	1.536
	Cell movement of dendritic cells	2.14E-08	1.360
	Migration of dendritic cells	5.03E-07	0.722
Cellular Movement, Immune Cell Trafficking	Cell movement of lymphatic system cells	3.37E-12	3.704
	Migration of lymphatic system cells	8.58E-12	3.584
Connective Tissue Development and Function, Tissue Development	Growth of connective tissue	1.43E-07	1.555
DNA Replication, Recombination, and Repair	Degradation of DNA	1.56E-06	1.920
	Metabolism of DNA	4.01E-08	1.785
Endocrine System Development and Function, Small Molecule Biochemistry	Metabolism of hormone	1.41E-06	1.063
Free Radical Scavenging	Production of reactive oxygen species	4.21E-07	3.161

Gastrointestinal Disease, Hepatic System Disease, Organismal Injury and Abnormalities	Liver lesion	7.06E-11	1.213
Gene Expression	Transcription	1.97E-10	4.334
	Transactivation	1.20E-11	4.152
	Expression of RNA	5.85E-12	4.151
	Transactivation of RNA	3.51E-11	3.966
	Transcription of RNA	9.73E-09	3.881
Infectious Diseases	Viral Infection	2.16E-26	7.212
	Infection by RNA virus	4.81E-16	6.617
	Infection of cells	3.80E-09	6.454
	HIV infection	3.36E-09	6.220
	Infection by HIV-1	2.10E-08	6.067
	Replication of RNA virus	2.70E-09	4.573
	Replication of virus	7.72E-10	4.326
Inflammatory Response	Inflammatory response	1.61E-13	4.332
	Immune response of cells	1.25E-15	1.872
	Inflammation of absolute anatomical region	1.44E-06	0.283
Inflammatory Response, Organismal Injury and Abnormalities	Inflammation of organ	5.07E-12	0.243
Organismal Injury and Abnormalities, Renal and Urological Disease	Renal lesion	9.75E-10	1.219
Organismal Survival	Organismal death	1.95E-09	1.376
	Survival of organism	1.70E-06	-1.000
Post-Translational Modification	Phosphorylation of protein	1.31E-06	3.486
Protein Degradation, Protein Synthesis	Catabolism of protein	1.60E-10	1.187
Protein Synthesis	Metabolism of protein	1.01E-13	1.059
Small Molecule Biochemistry	Biosynthesis of amide	5.62E-07	2.064
Tissue Development	Growth of epithelial tissue	5.70E-10	2.361
	Development of epithelial tissue	1.52E-07	2.319
Tissue Morphology	Quantity of cells	1.60E-07	1.260

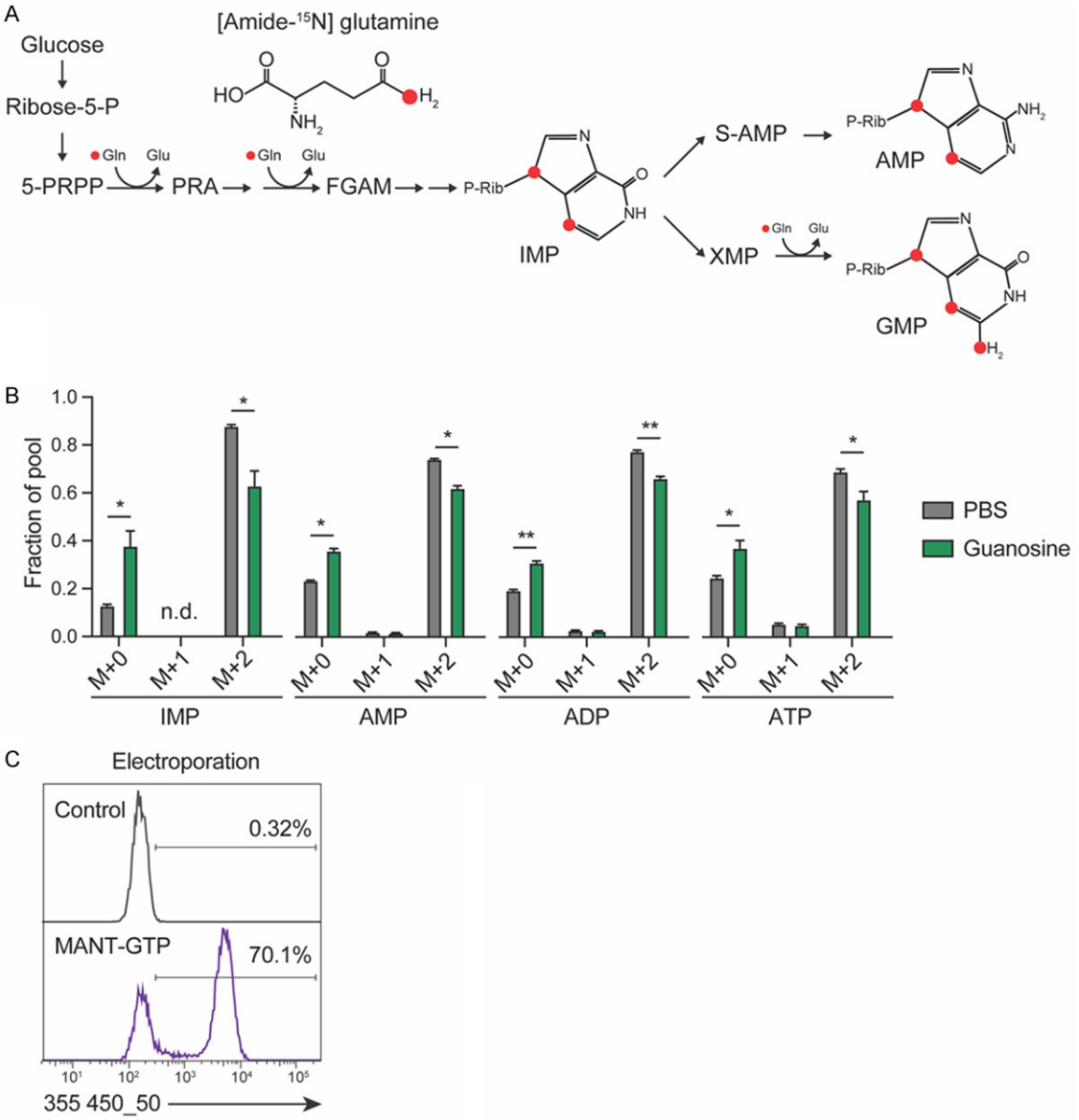

Supplementary Figure 2. Guanosine promotes differentiation through intracellular GTP accumulation. (Related to **Figure 4**) A. Schematic illustration of [amide-^{15}N] glutamine labeling pattern. Ribose-5-P, ribose 5'-phosphate; 5-PRPP, 5'-phosphoribosyl pyrophosphate; PRA, 5'-phosphoribosylamine; FGAM, 5'-phosphoribosylformylglycinamidine; IMP, inosine monophosphate; S-AMP, adenylosuccinate; AMP, adenosine monophosphate; XMP, xanthosine monophosphate; GMP, guanosine monophosphate; Gln, glutamine; Glu, glutamate; Asp, aspartate. B. Fractional labeling of IMP, AMP, ADP, and ATP in guanosine-treated or control U937 cells cultured in media containing [amide-^{15}N] glutamine for 12 hours. M+2 was the dominant labeled form. Data are presented as mean ± SD from duplicates. *P<0.05, **P<0.01 as assessed by student's t test. C. U937 cells were electroporated with nucleofector solution buffer containing 1 mM MANT-GTP or vehicle control followed by flow cytometry analysis via 355 450_50 channel. The percentages of MANT-GTP^{+} gate are shown.

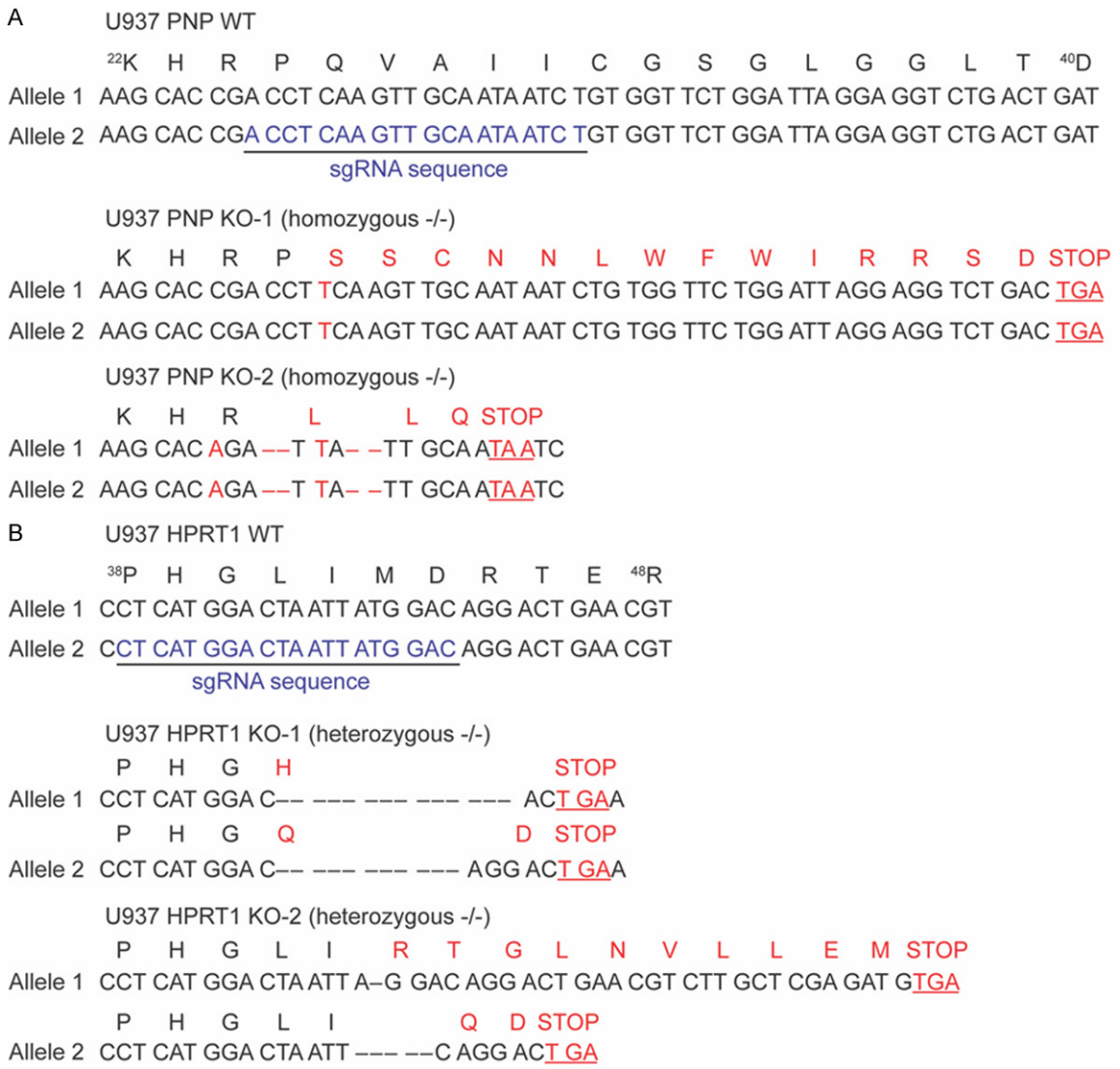

Supplementary Figure 3. Genotype of PNP or HPRT1 KO cell clones. (Related to **Figures 5**, **6**) A. Genotyping of U937 PNP KO single cell clones demonstrates biallelic homozygous truncations. sgRNA sequence is highlighted in blue. B. Genotyping of U937 HPRT1 KO single cell clones demonstrates biallelic heterozygous truncations. sgRNA sequence is highlighted in blue.